Electronic Supplementary Information

Electron-donating curved π-electronic systems that complex with buckyball

Hiromitsu Maeda,* Taichi Abiko, Yohei Haketa, Yoichi Kobayashi, Yukihide Ishibashi, Tsuyoshi Asahi and Nobuhiro Yasuda

Department of Applied Chemistry, College of Life Sciences, Ritsumeikan University, Kusatsu 525–8577, Japan, Fax: +81 77 561 2659; Tel: +81 77 561 5969; E-mail: maedahir@ph.ritsumei.ac.jp, *Department of Materials Science and Biotechnology, Graduate School of Science and Engineering, Ehime University, Matsuyama 790–8577, Japan and Diffraction and Scattering Division, Japan Synchrotron Radiation Research Institute, Sayo 679–5198, Japan*

Table of contents

1. Spectroscopic data

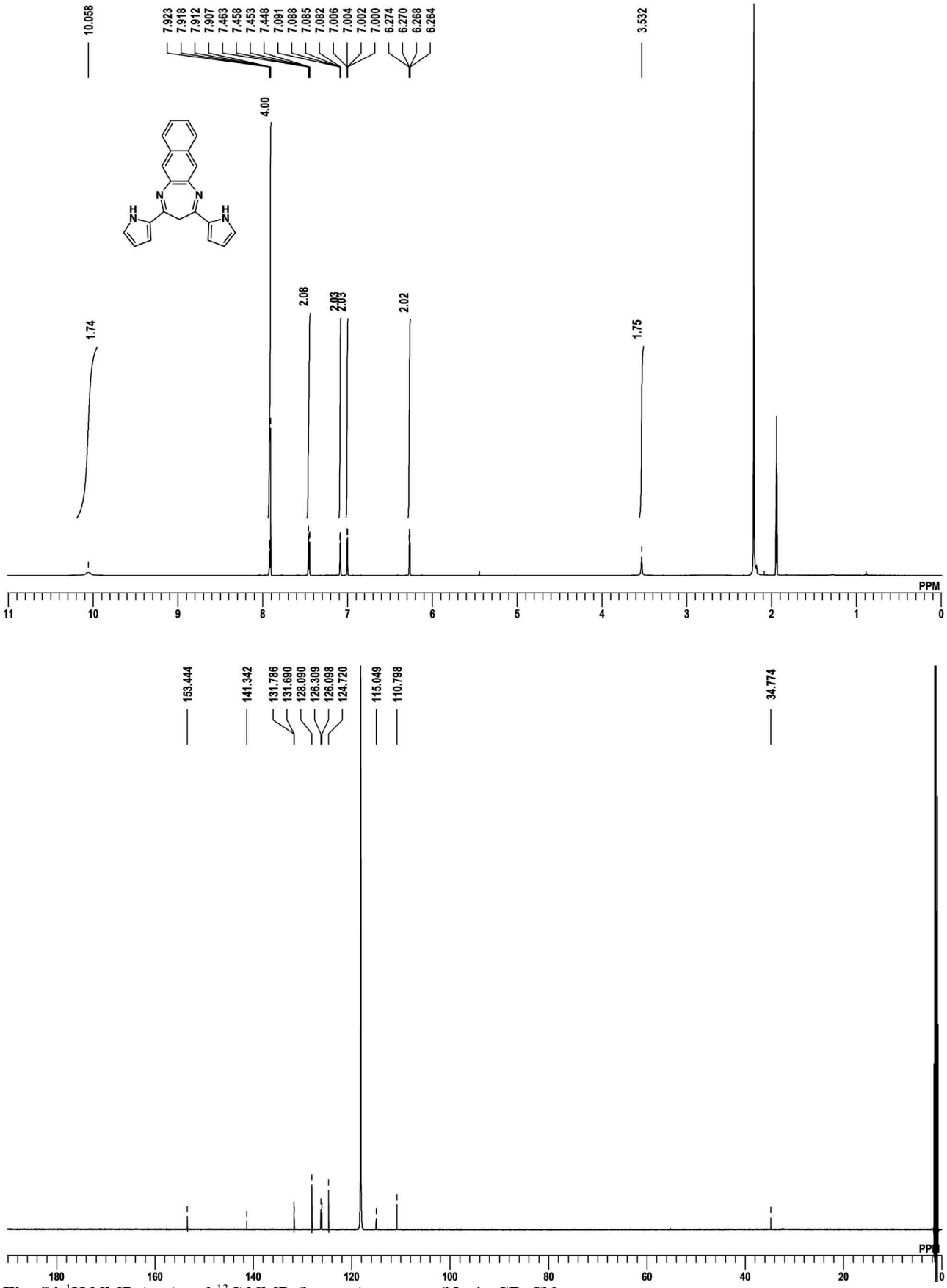

Fig. S1 ^{1}H NMR (top) and ^{13}C NMR (bottom) spectra of **2a** in CD_3CN.

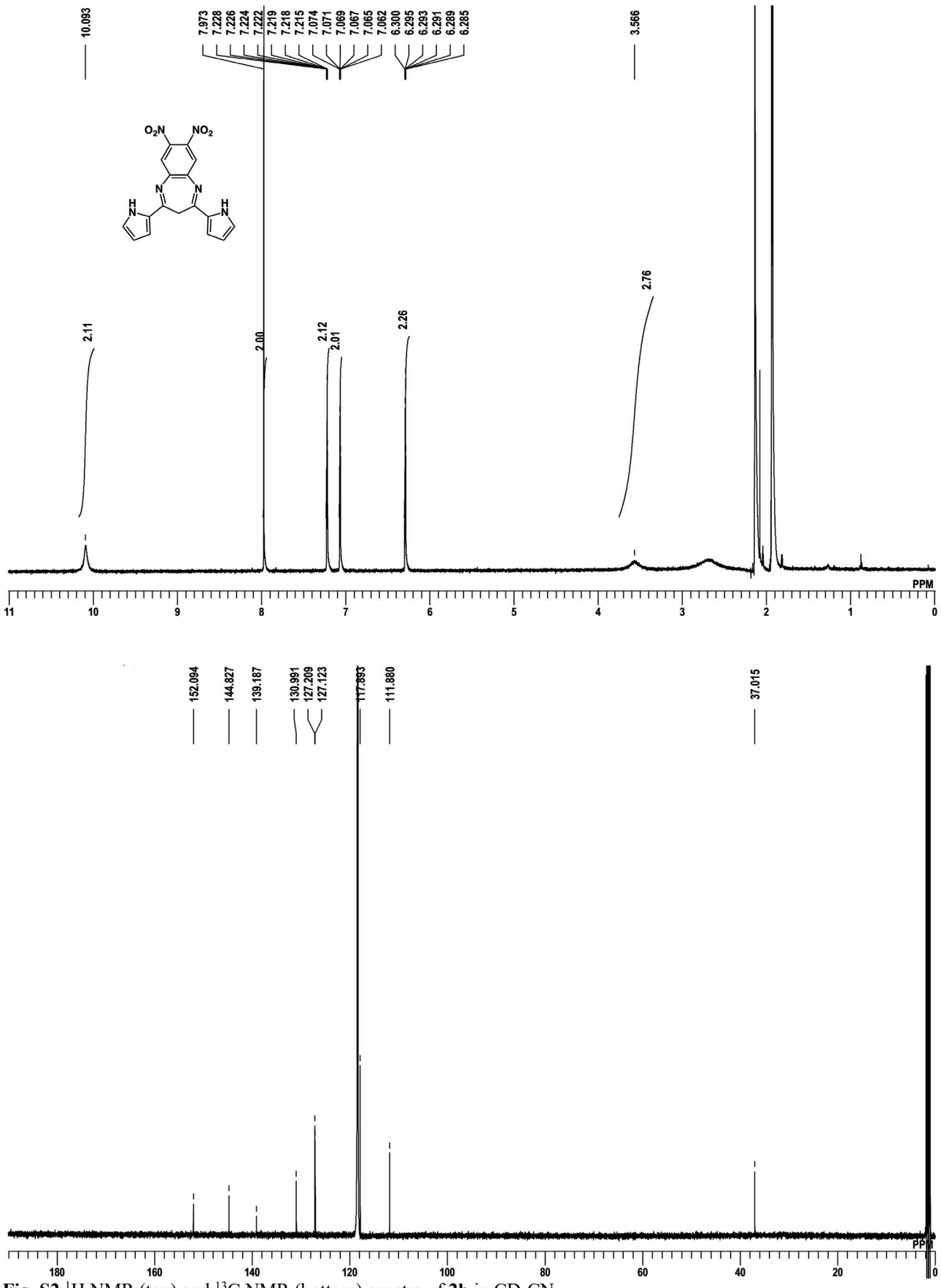

Fig. S2 ^{1}H NMR (top) and ^{13}C NMR (bottom) spectra of **2b** in CD_3CN.

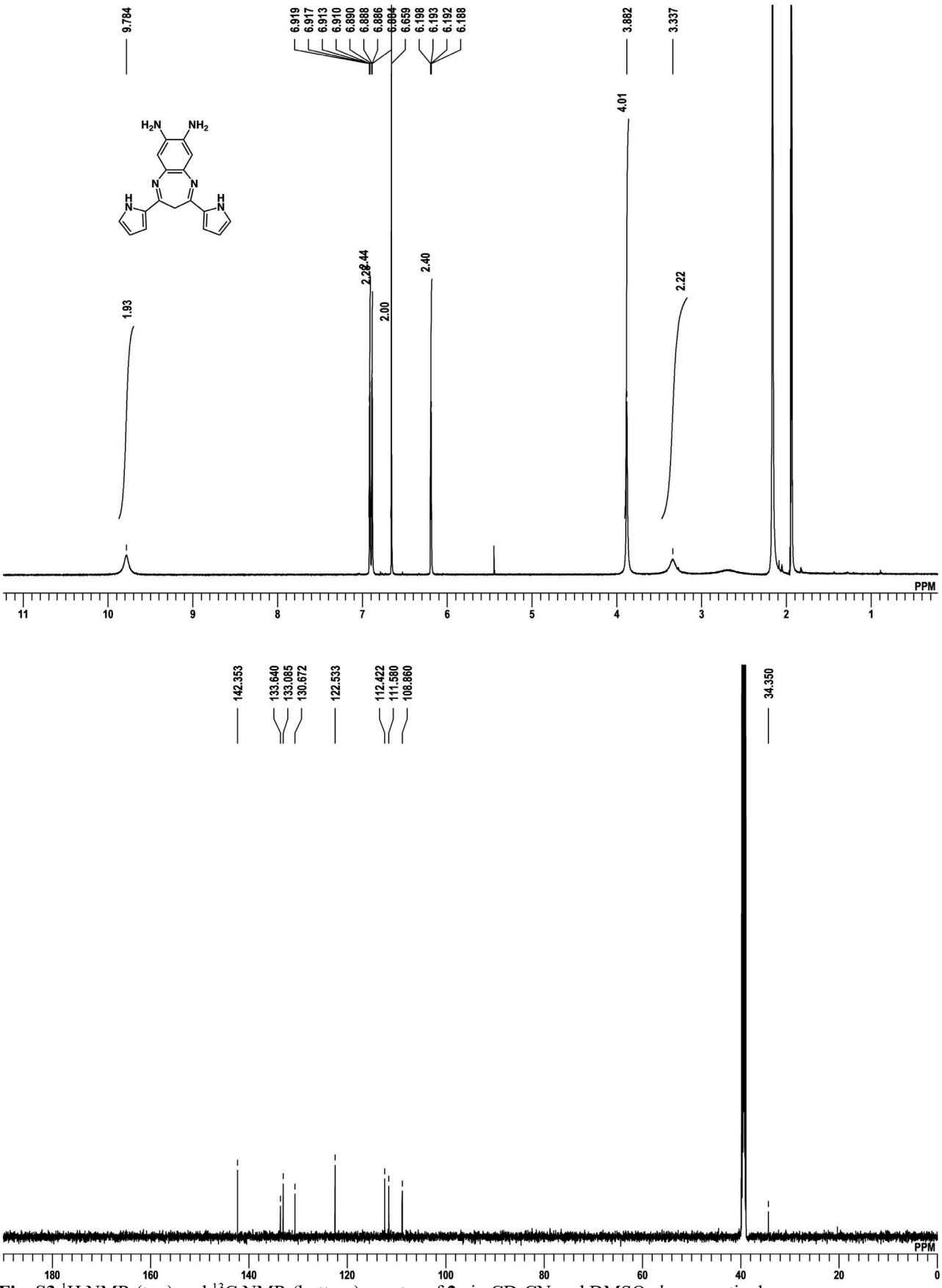

Fig. S3 ^{1}H NMR (top) and ^{13}C NMR (bottom) spectra of **2c** in CD_3CN and DMSO-d_6, respectively.

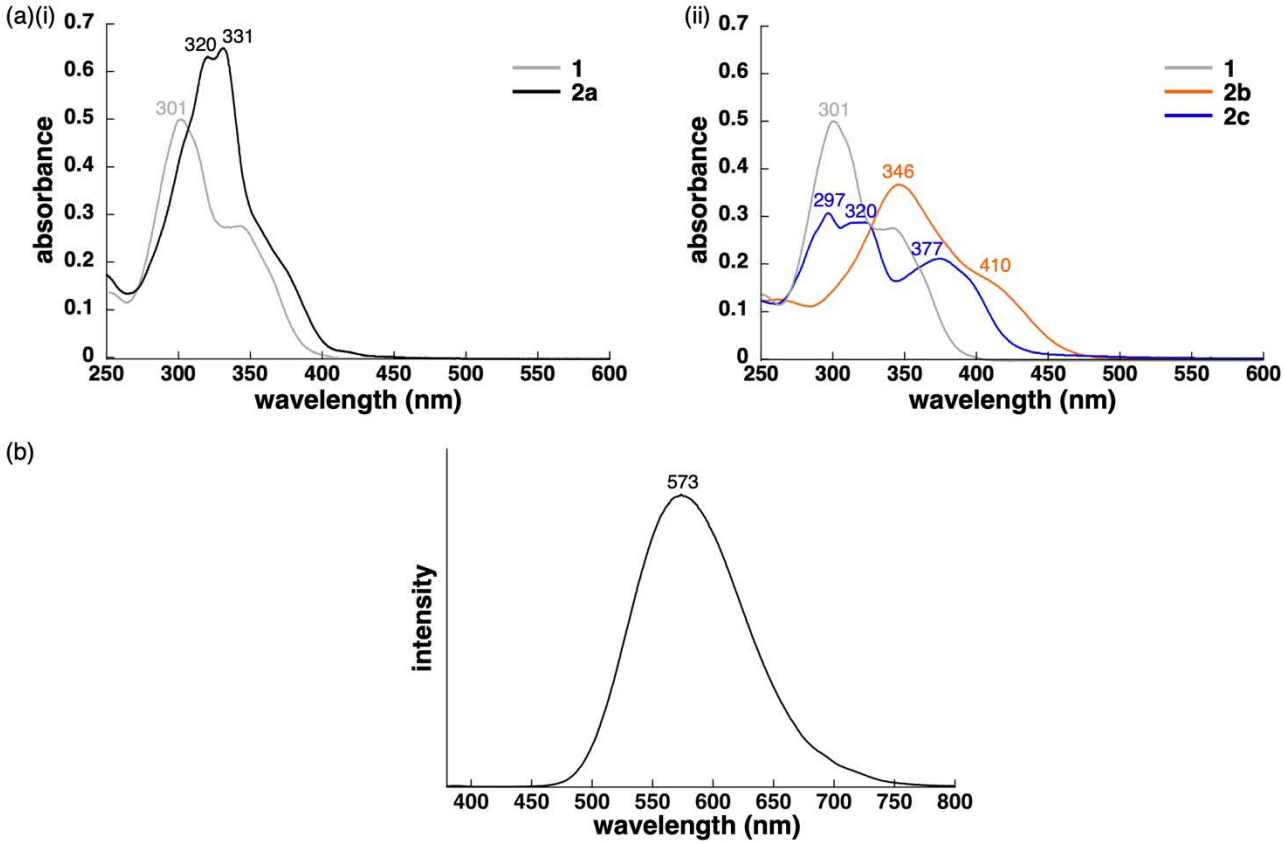

Fig. S4 (a) UV/vis absorption spectra of (i) **2a** and (ii) **2b** (red) and **2c** (blue) in CH_2Cl_2 (1×10^{-5} M) along with that of dpb **1**[S1] (gray) as a reference and (b) fluorescence spectrum of **2b** excited at the absorption maximum in CH_2Cl_2 (1×10^{-5} M). Fluorescence spectra of **2a**,**c** are not shown due to the very weak fluorescence intensities.

[S1] Y. Haketa, M. Miyasue, Y. Kobayashi, R. Sato, Y. Shigeta, N. Yasuda, N. Tamai and H. Maeda, H. *J. Am. Chem. Soc.*, 2020, **142**, 16420–16428.

2. X-ray crystallographic data

Table S1 Crystallographic details.

	2b	**2c**	**2c´**	**2a**$_6$·C_{60}
formula	$C_{17}H_{12}N_6O_4$	$C_{17}H_{16}N_6$·2.79H_2O	$C_{28}H_{22}N_8$·2C_3H_6O	6$C_{21}H_{16}N_4$·C_{60}
fw	364.33	354.71	586.69	2666.86
crystal size, mm	0.600 × 0.093 × 0.093	0.16 × 0.02 × 0.01	0.05 × 0.05 × 0.02	0.02 × 0.02 × 0.01
crystal system	monoclinic	monoclinic	monoclinic	orthorhombic
space group	$P2_1/n$ (no. 14)	$C2/c$ (no. 15)	$P2/c$ (no. 13)	$Pmna$ (no. 53)
a, Å	10.3729(16)	18.6232(7)	17.0114(15)	22.9648(4)
b, Å	13.246(2)	4.9442(2)	10.6570(9)	10.6622(2)
c, Å	11.8907(18)	37.5921(15)	16.6958(15)	25.4143(5)
α, °	90	90	90	90
β, °	103.755(7)	100.107(2)	99.207(3)	90
γ, °	90	90	90	90
V, Å^3	1586.9(4)	3407.6(2)	2987.8(5)	6222.8(2)
ρ_{calcd}, g cm^{-3}	1.525	1.383	1.304	1.423
Z	4	8	4	2
T, K	100(2)	90(2)	90(2)	90(2)
μ, mm^{-1}	0.045 [a]	0.131 [a]	0.085 [b]	0.113 [a]
no. of reflns	35250	16622	27161	63517
no. of unique reflns	3642	3095	4787	5856
variables	245	272	401	479
λ, Å	0.4125 [a]	0.81106 [a]	0.71073 [b]	0.81106 [a]
R_1 ($I > 2\sigma(I)$)	0.0331	0.0486	0.0678	0.0917
wR_2 ($I > 2\sigma(I)$)	0.0897	0.1217	0.1545	0.2000
GOF	1.044	1.062	1.049	1.117

[a] Synchrotron radiation. [b] Mo-Kα radiation.

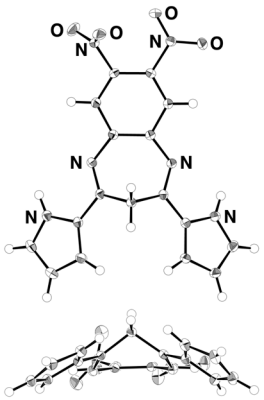

Fig. S5 Ortep drawing of single-crystal X-ray structure (top and side views) of **2b**. Thermal ellipsoids are scaled to the 50% probability level.

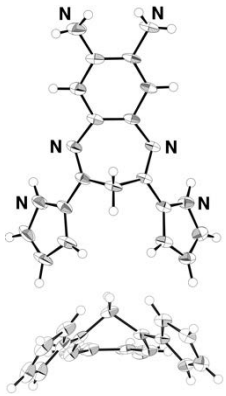

Fig. S6 Ortep drawing of single-crystal X-ray structure (top and side views) of **2c**. Thermal ellipsoids are scaled to the 50% probability level. Solvent molecules are omitted for clarity.

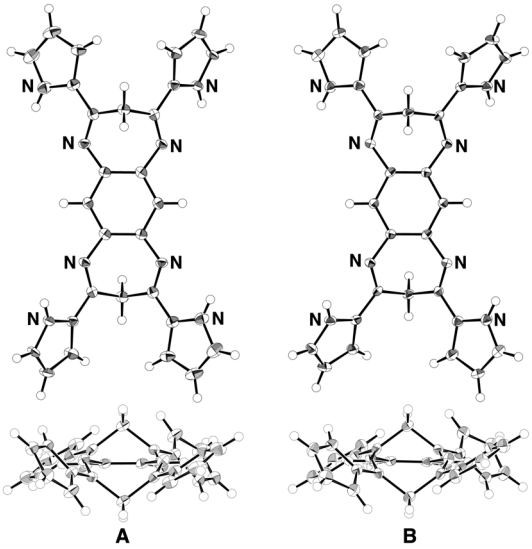

Fig. S7 Ortep drawing of single-crystal X-ray structure (top and side views) of **2c´** as two independent structures (Forms A and B). Thermal ellipsoids are scaled to the 50% probability level. Solvent molecules are omitted for clarity.

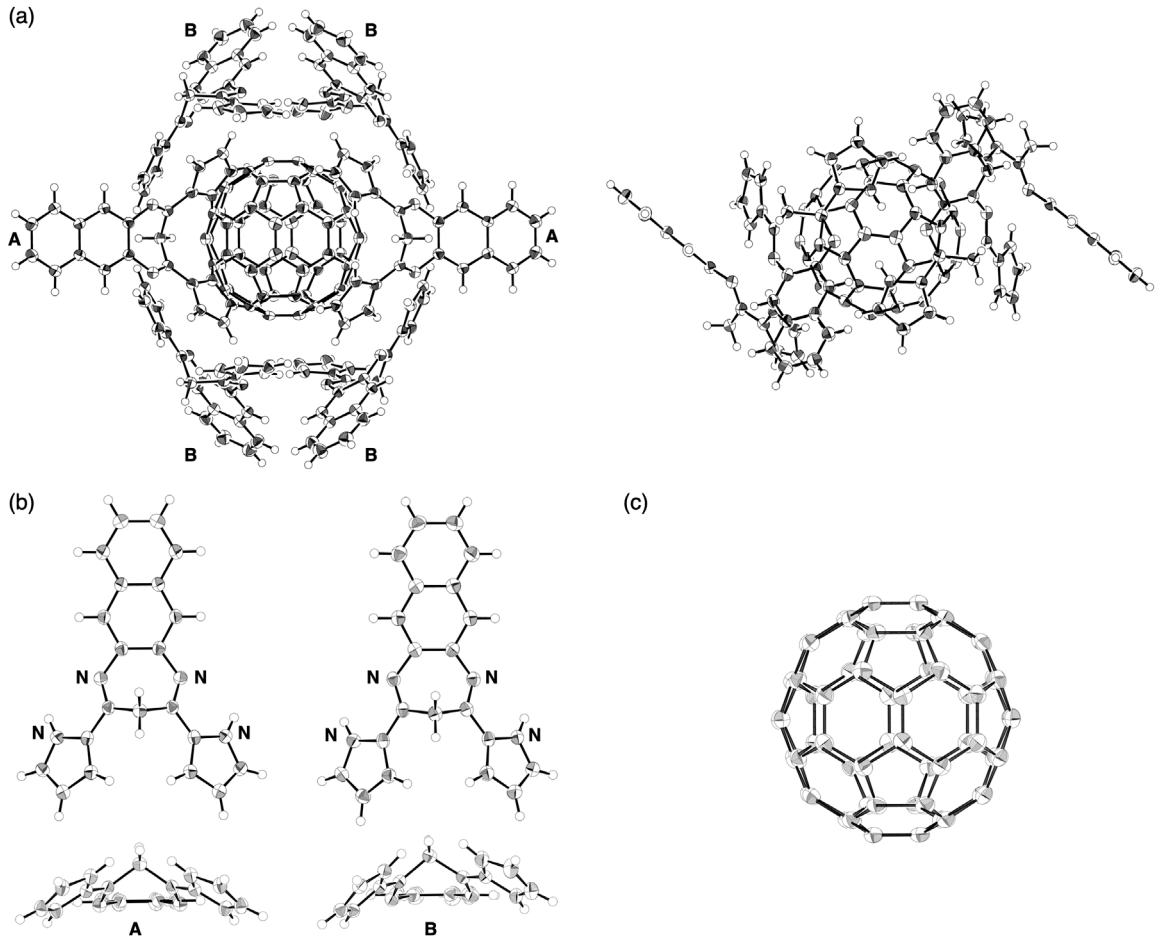

Fig. S8 Ortep drawing of single-crystal X-ray structure of **2a**$_6$·C_{60} as (a) a whole structure (top and side views), (b) constituent **2a** as independent structures (Forms A and B) (top and side views), and (c) constituent C_{60}. Thermal ellipsoids are scaled to the 50% probability level.

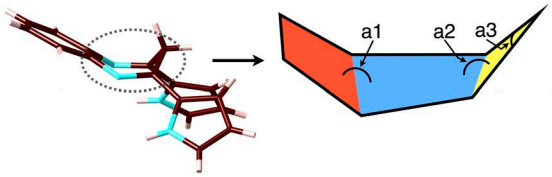

Fig. S9 Definition of the dihedral angles a1 and a2 and the C–C–C angle a3 at CH_2 unit in the seven-membered ring.

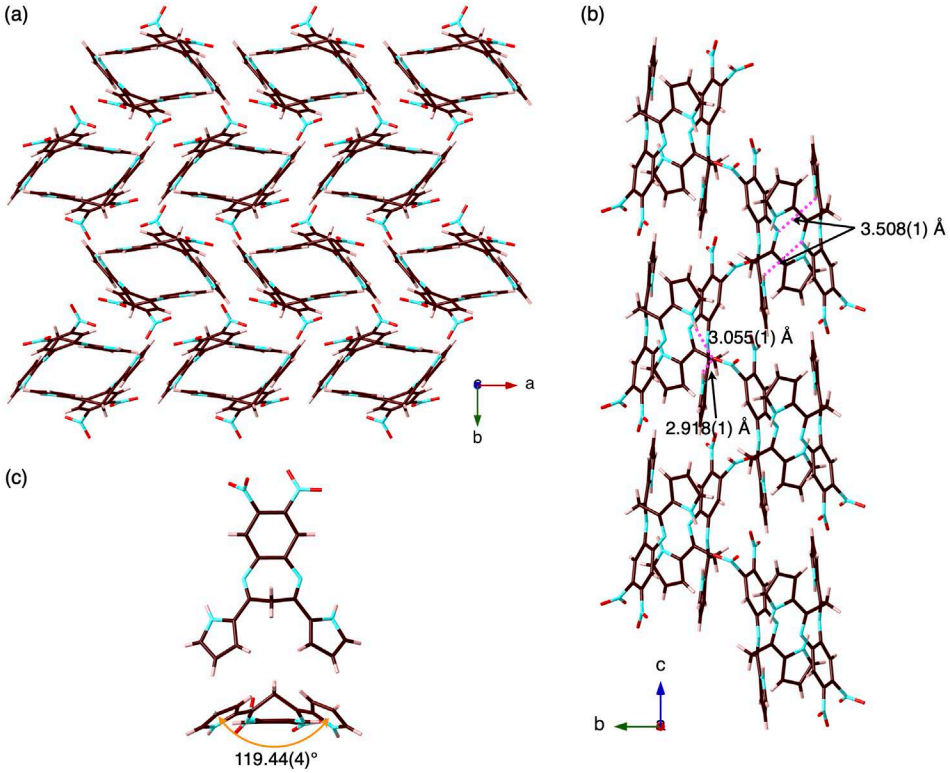

Fig. S10 Single-crystal X-ray structure of **2b**: packing diagrams through (a) *c* and (b) *a* axes of **2b** and (c) monomer, forming hydrogen-bonding assembly with the N(–H)···N distance of 3.508(1) Å and the N(–H)···O distances of 2.918(1)/3.055(1) Å. Angles a1, a2, and a3 (Fig. S9) in the seven-membered ring are 147.97(4)°, 125.68(9)°, and 107.09(8)°, respectively, whereas the dihedral angle between two pyrrole rings is 119.44(4)°. Atom color code: brown, pink, blue, and red refer to carbon, hydrogen, nitrogen, and oxygen, respectively.

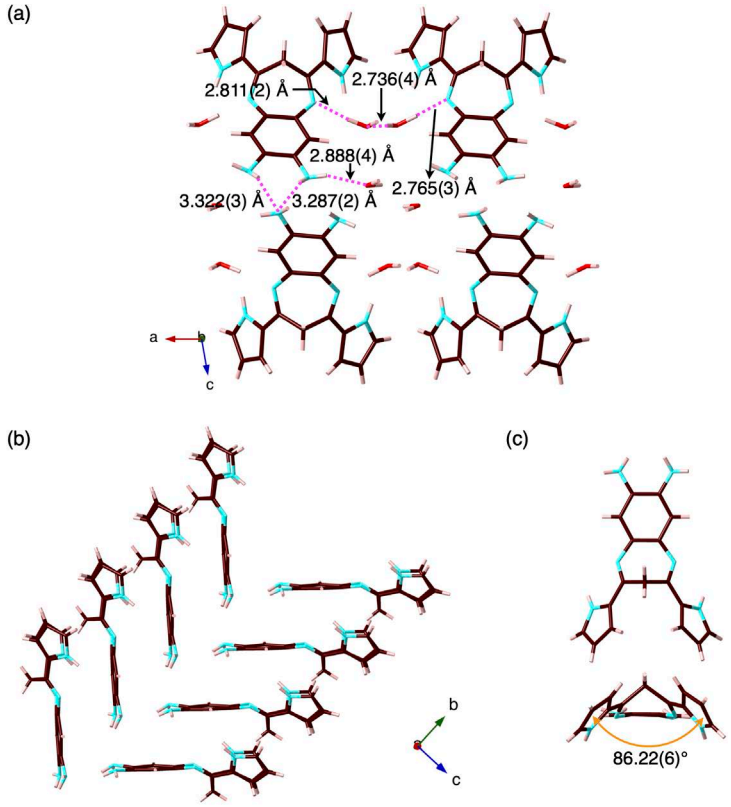

Fig. S11 Single-crystal X-ray structure of **2c**: packing diagrams through (a) *b* and (b) *a* axes of **2c** and (c) monomer, forming hydrogen-bonding assembly with the N(–H)···N distance of 3.287(2)/3.322(3) Å. Angles a1, a2, and a3 (Fig. S9) in the seven-membered ring are 144.70(12)°, 121.95(12)°, and 104.19(14)°, respectively, whereas the dihedral angle between two pyrrole rings is 86.22(6)°. Atom color code: brown, pink, blue, and red refer to carbon, hydrogen, nitrogen, and oxygen, respectively. In (a), minor disorder water molecules are omitted for clarity, whereas, in (b), solvent molecules are omitted for clarity.

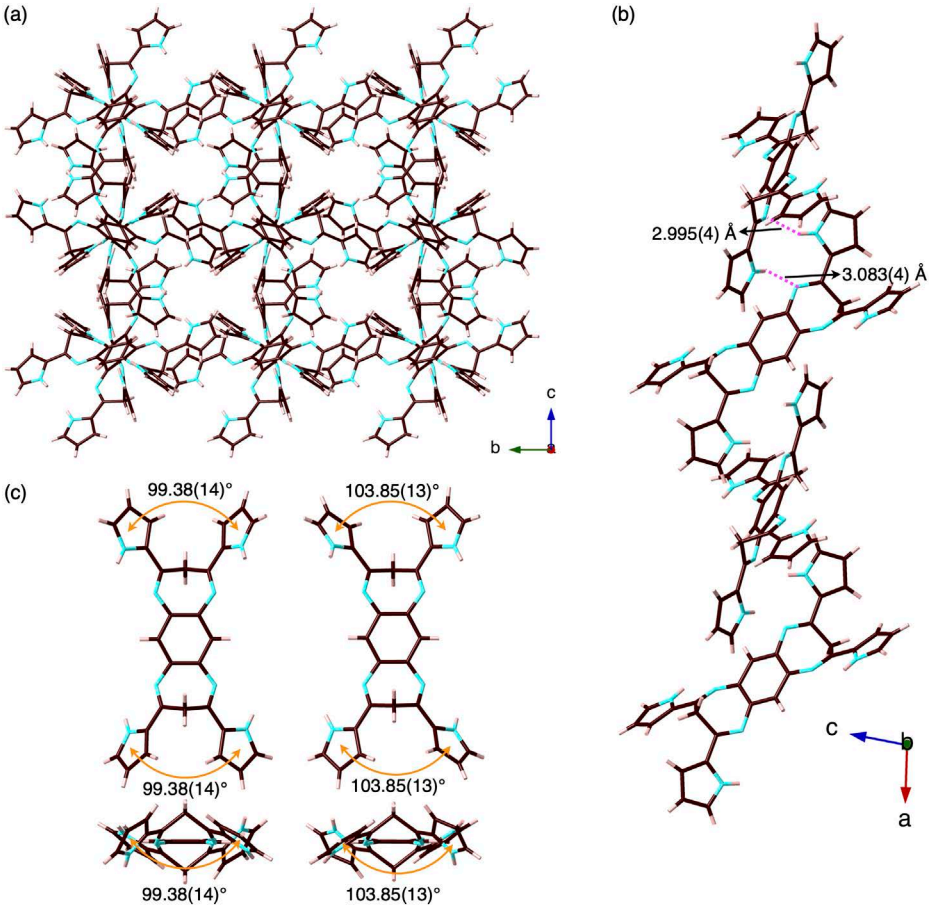

Fig. S12 Single-crystal X-ray structure of **2c´**: packing diagrams through (a) *a* and (b) *b* axes of **2c´** and (c) monomer, forming a hydrogen-bonding 1D chain assembly with the N(–H)···N distances of 3.00/3.08 Å. Angles a1, a2, and a3 (Fig. S9) in the seven-membered rings of two independent structures are 144.53(14)°, 123.72(26)°, and 104.4(3)°and 144.08(17)°, 123.87(23)°, and 105.4(2)°, whereas the dihedral angles between two pyrrole rings are 99.38(14)° and 103.85(13)°. Atom color code: brown, pink, and blue refer to carbon, hydrogen, and nitrogen, respectively. Solvent molecules are omitted for clarity.

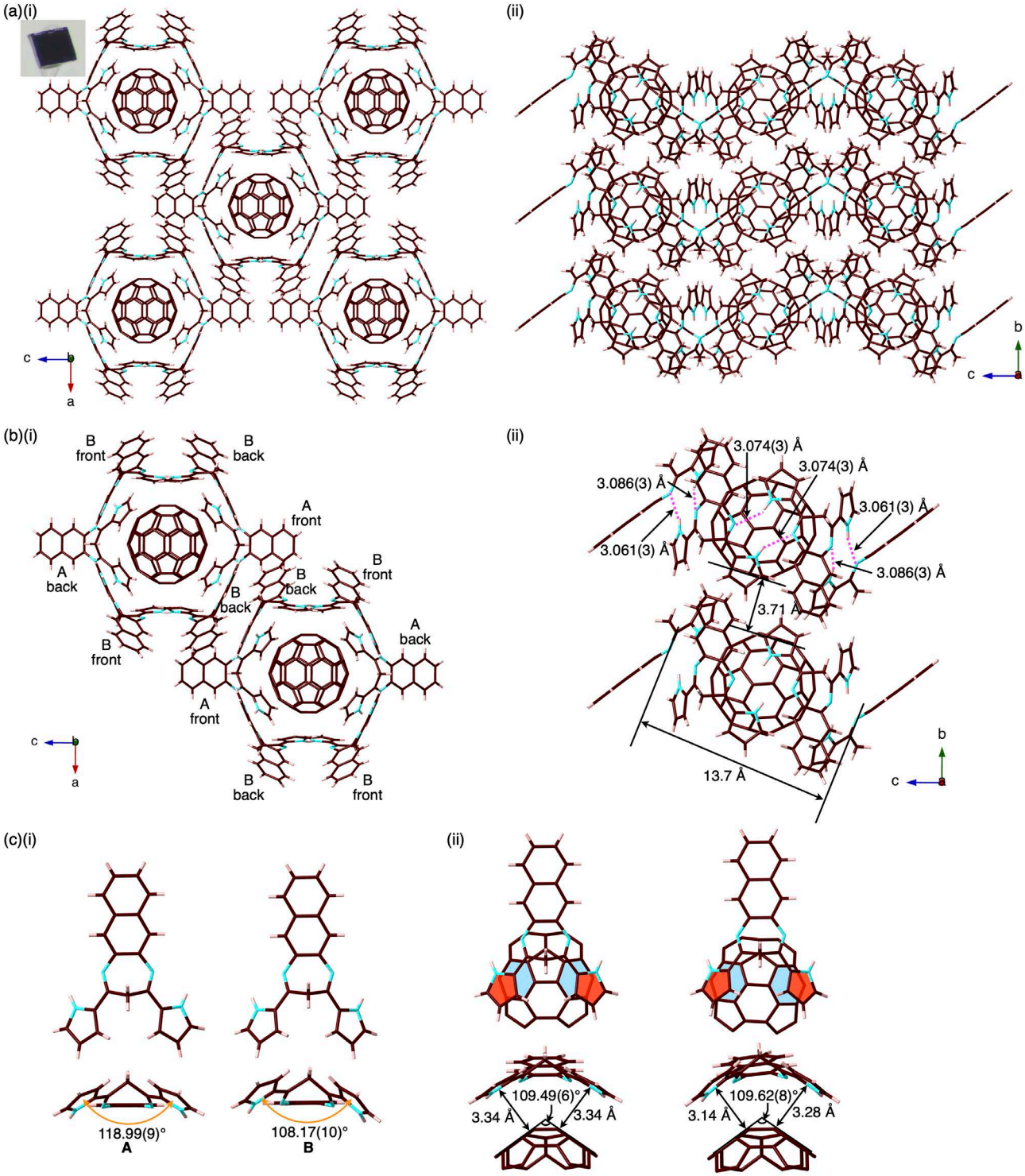

Fig. S13 Packing diagrams of **2a**$_6$·C_{60}: (a)(i) top and (ii) side views of columns (inset: photograph of the crystal viewed from the *b*-axis), (b)(i) top view (the labels of front and back indicate the locations of benzo units) and (ii) side view of a column, and (c)(i) monomers of **2a**, wherein Forms A and B of **2a** correspond to Forms A and B, respectively, in Fig. S8, forming a hydrogen-bonding cyclic structure with the N(–H)···N distances of 3.061(3)/3.074(3)/3.086(3) Å and (ii) top and side views of **2a** with a partial structure of C_{60} (stacking five- and six-membered rings are colored with red and blue, respectively). Through the crystal indexing, the **2a**$_6$·C_{60} units were aligned to form columnar structures along the *b*-axis as the short side of the plate crystal. Angles a1, a2, and a3 (Fig. S9) in the seven-membered rings are 142.61(23)°, 125.15(20)°, and 107.3° for Form A, 142.44(12)°, 124.48(18)°, and 107.22(18)° for Form B, respectively. Dihedral angles between two pyrrole rings in Forms A and B are 118.99(9)° and 108.17(10)°, respectively, whereas those of C_{60} six-membered rings stacking with the pyrrole rings are 109.49(6)° and 109.62(8)°, respectively. Distances between C_{60} six-membered rings and pyrrole rings are 3.34 Å for Form A and 3.14 and 3.28 Å for Form B. Atom color code: brown, pink, and blue refer to carbon, hydrogen, and nitrogen, respectively.

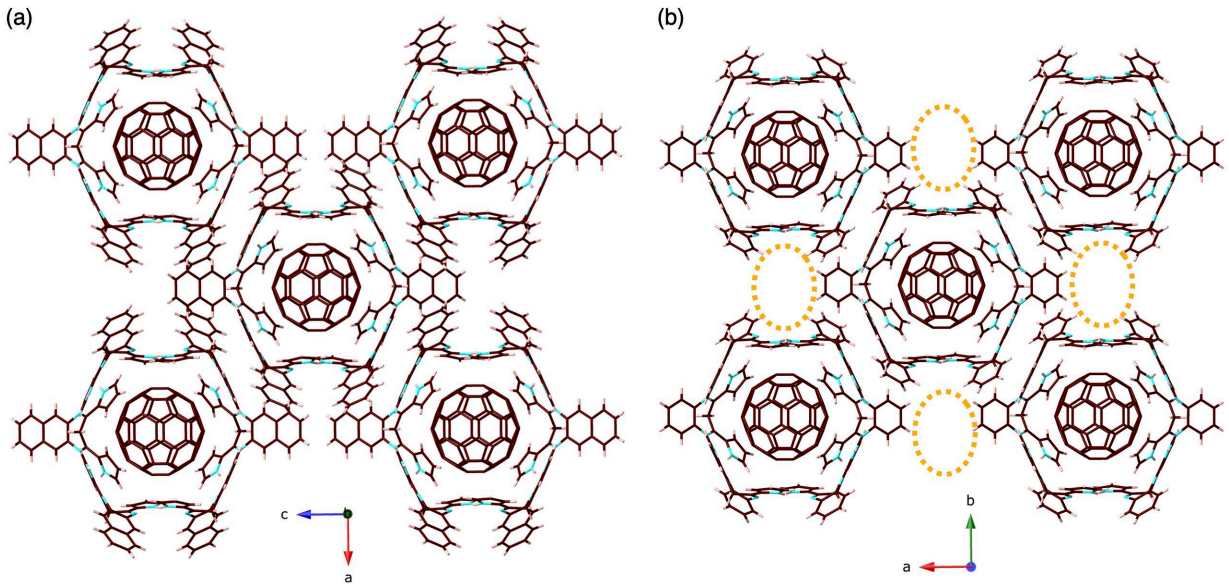

Fig. S14 Comparison diagrams of the single-crystal X-ray structures of (a) **2a**$_6$·C_{60} and (b) **1**$_6$·C_{60}.[S2] It is noteworthy that, in (b), crystallizing solvent molecules, $CHCl_3$ and *n*-hexane, are included in the void indicated by orange broken line circles in the ratio of 1.35:0.52, whereas, in (a), no solvent molecules are not observed due to the smaller void by the naphthyl units.

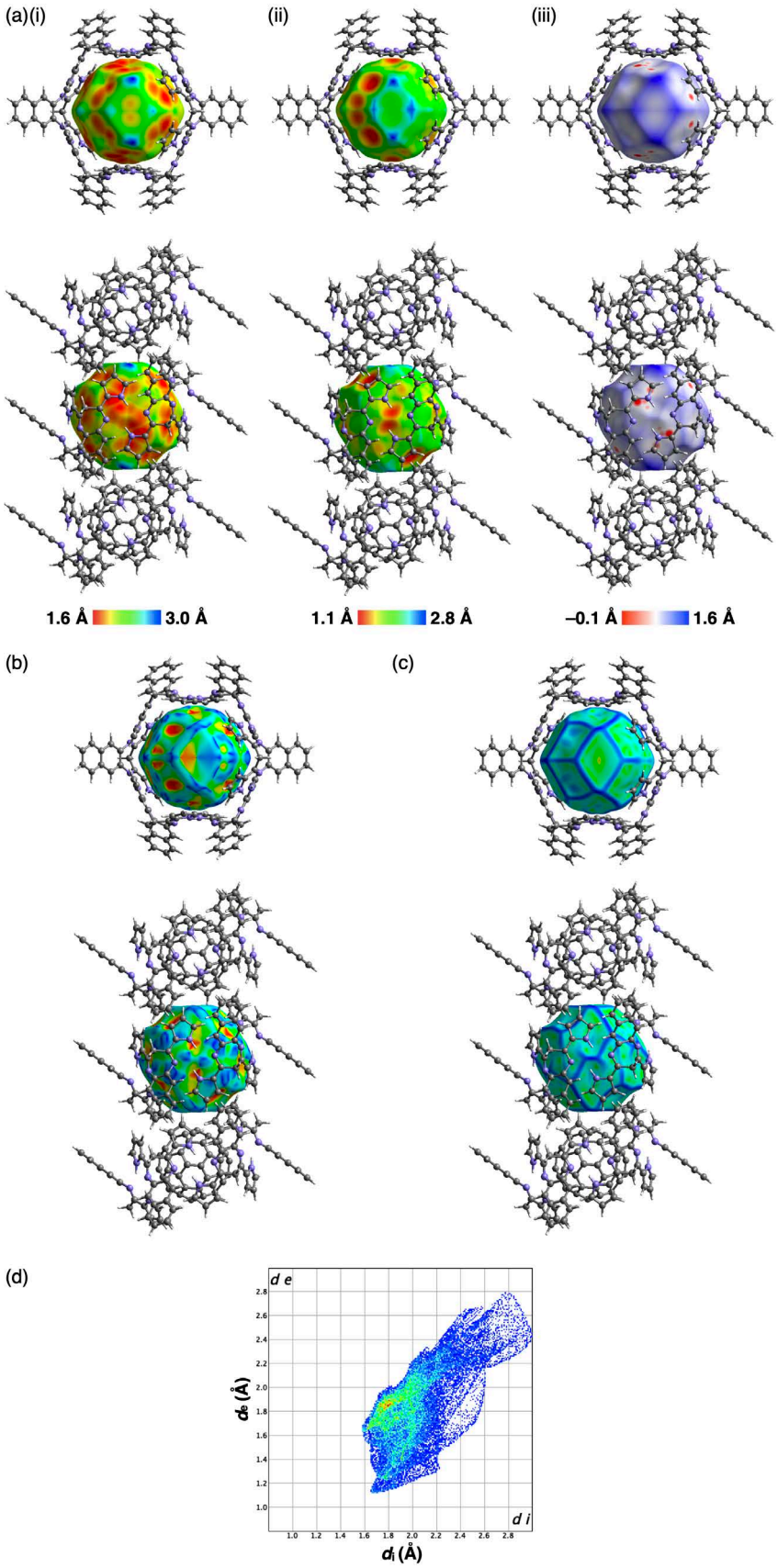

Fig. S15 Hirshfeld surfaces[S2] of C_{60} in **2a**$_6$·C_{60} from the crystal structure (Fig. S8,13): (a) mapped with (i) d_i, (ii) d_e, and (iii) d_{norm} (top and side views), (b) mapped with shape index, (c) mapped with curvedness, and (d) fingerprint plot (d_i and d_e). Solvent molecules with disorders are omitted for clarity. Atom color code in (a,b): gray, white, and blue refer to carbon, hydrogen, and nitrogen, respectively. Hirshfeld surface mapped with d_e shows intercomplex CH–π interactions between pyrrole β-CH and C_{60}. Furthermore, shape index exhibits red and blue triangles arranged in bow-tie shape, indicating the π–π stackings of pyrrole ring and six-membered ring of C_{60}.

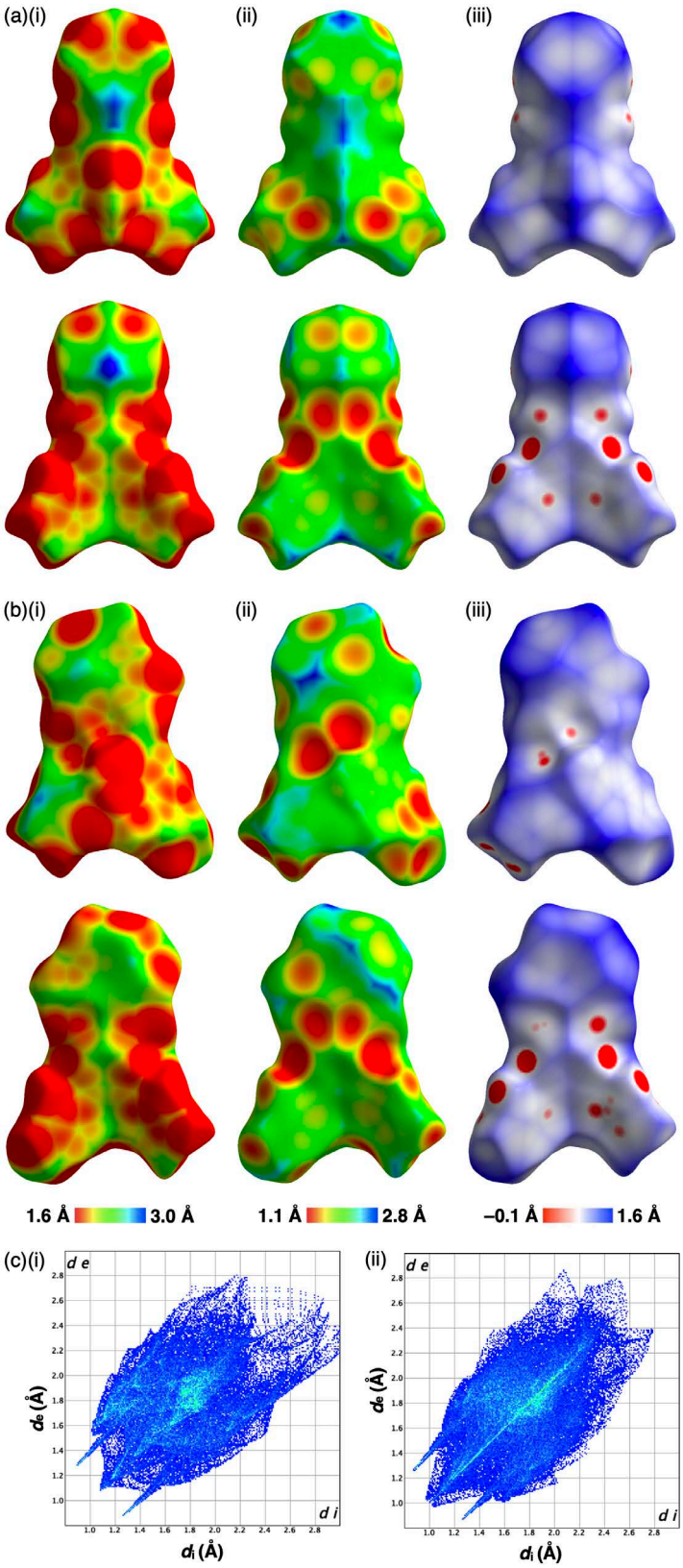

Fig. S16 Hirshfeld surfaces[S2] of **2a** in **2a**$_6$·C_{60} from the crystal structure (Fig. S8,13): (a) Form A and (b) Form B mapped with (i) d_i, (ii) d_e, and (iii) d_{norm} (concave and convex views) and (c) fingerprint plots (d_i and d_e) of (i) Form A and (ii) Form B. Hirshfeld surface mapped with d_e indicates hydrogen bonding between pyrrole NH and benzodiazepine N.

[S2] P. R. Spackman, M. J. Turner, J. J. McKinnon, S. K. Wolff, D. J. Grimwood, D. Jayatilaka and M. A. Spackman, *J. Appl. Cryst.*, 2021, **54**, 1006–1011.

3. Theoretical studies

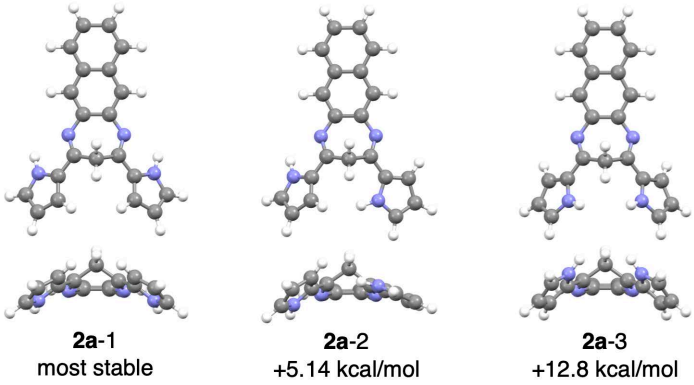

Fig. S17 Optimized structures (top and side views) of **2a** at B3LYP/6-31G(d,p).

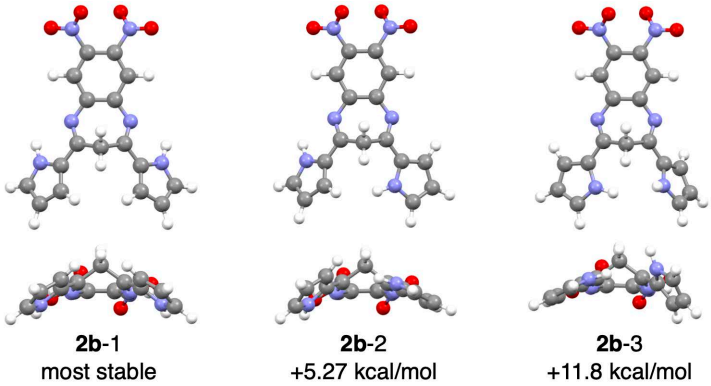

Fig. S18 Optimized structures (top and side views) of **2b** at B3LYP/6-31G(d,p).

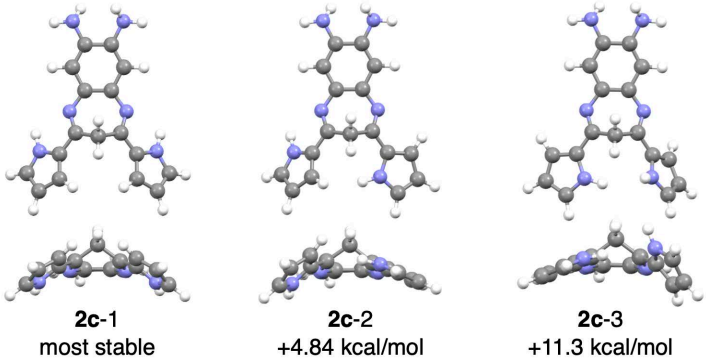

Fig. S19 Optimized structures (top and side views) of **2c** at B3LYP/6-31G(d,p).

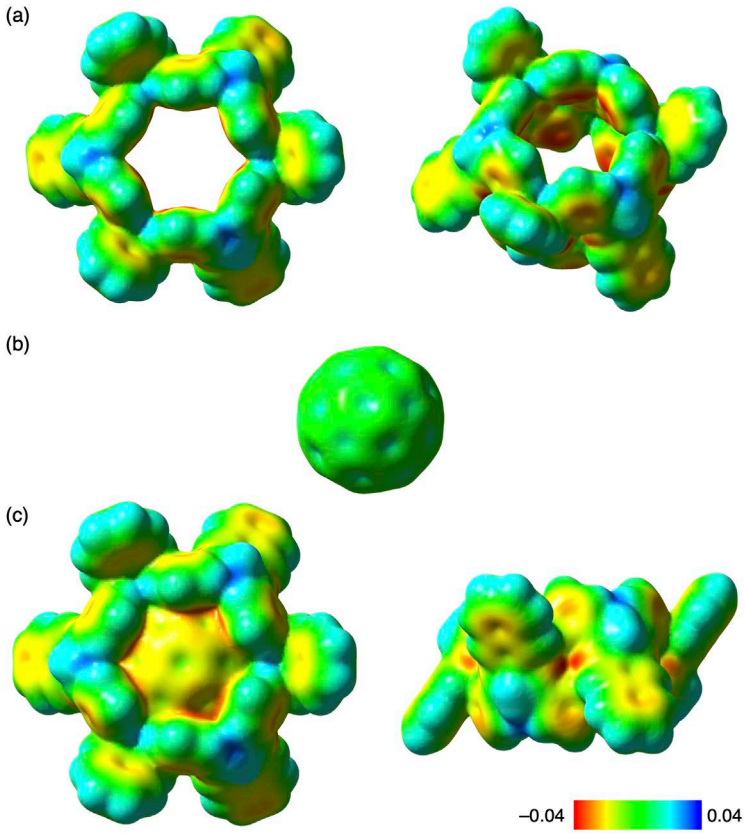

Fig. S20 Electrostatic potentials (ESP) mapped onto the electron density isosurfaces (δ = 0.001) of **2a**$_6$·C_{60} at B3LYP/6-31G(d,p) based on the crystal structure (Fig. S13): (a) **2a**$_6$, (b) C_{60}, and (c) **2a**$_6$·C_{60}. Inner surface of **2a**$_6$ ring structure shows relatively higher electron density than the outer surface. Higher electron density of C_{60} in **2a**$_6$·C_{60} than C_{60} alone was observed, indicating the effective π–π stacking interaction between electron-rich pyrrole and relatively electron-deficient C_{60}.

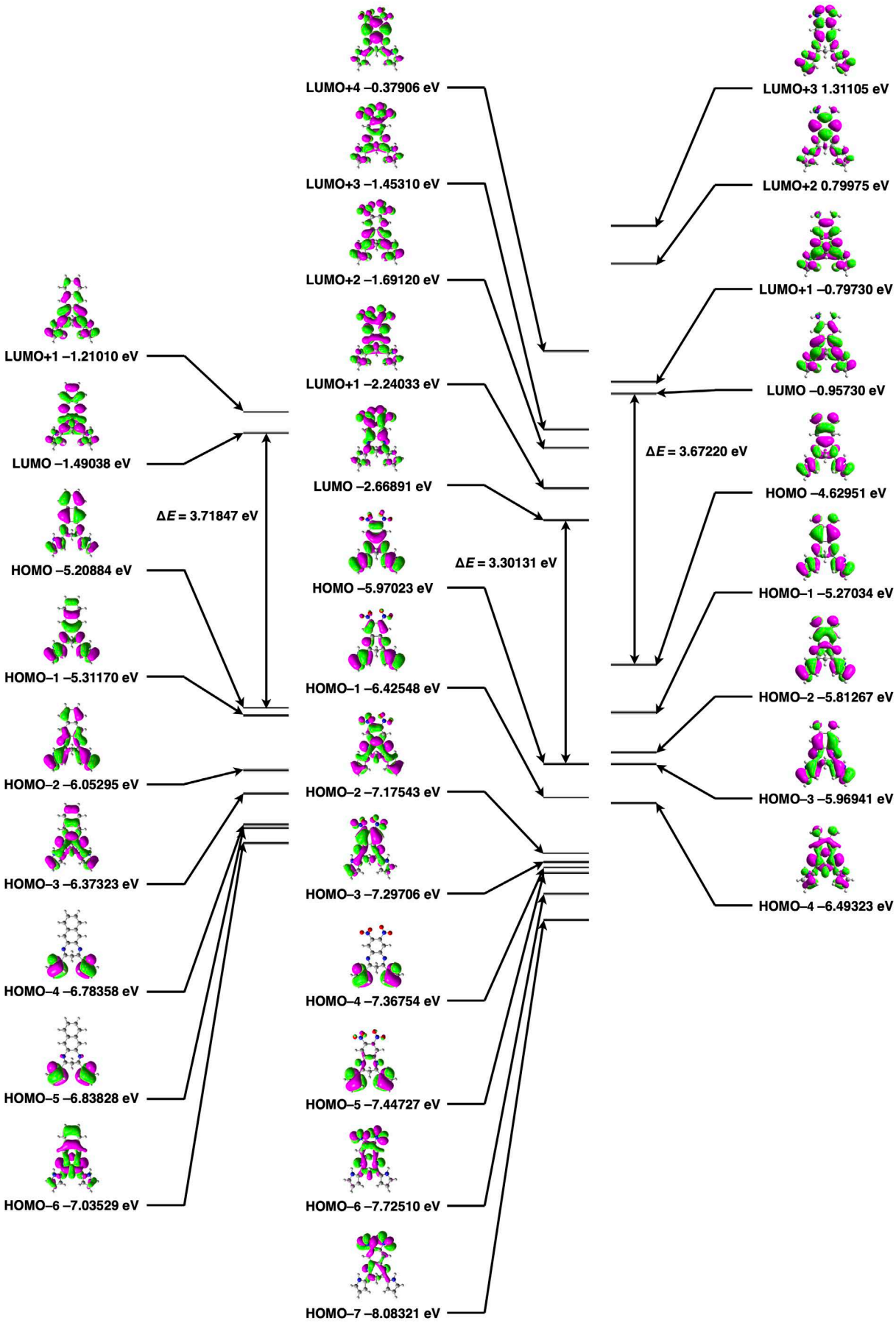

Fig. S21 Molecular orbitals (HOMO/LUMO) of **2a** (left), **2b** (middle), and **2c** (right) estimated at B3LYP/6-31G(d,p) level.

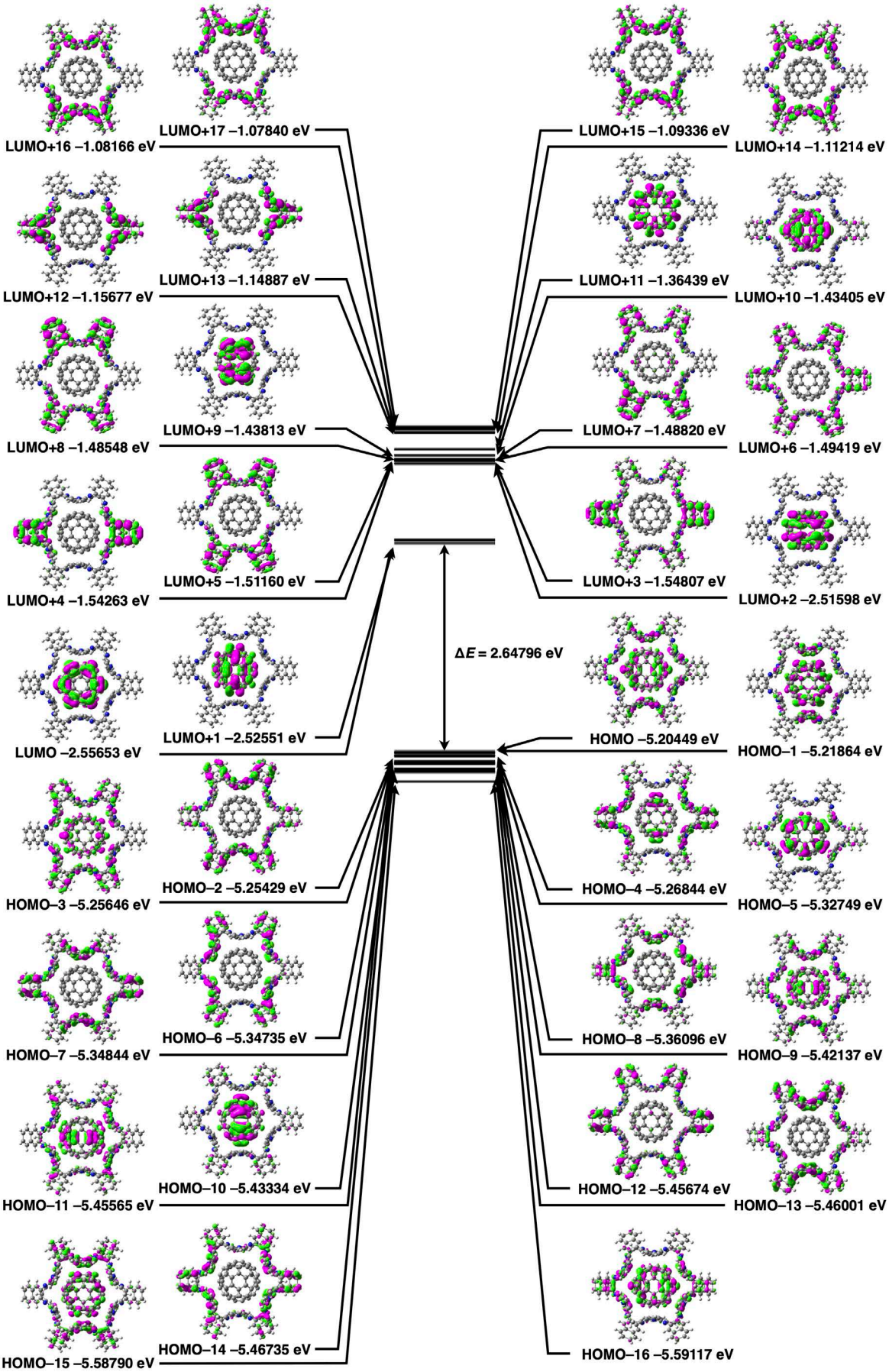

Fig. S22 Molecular orbitals (HOMO/LUMO) of **2a**$_6$·C_{60} estimated at B3LYP/6-31G(d,p) based on the crystal structure (Fig. S8,13).

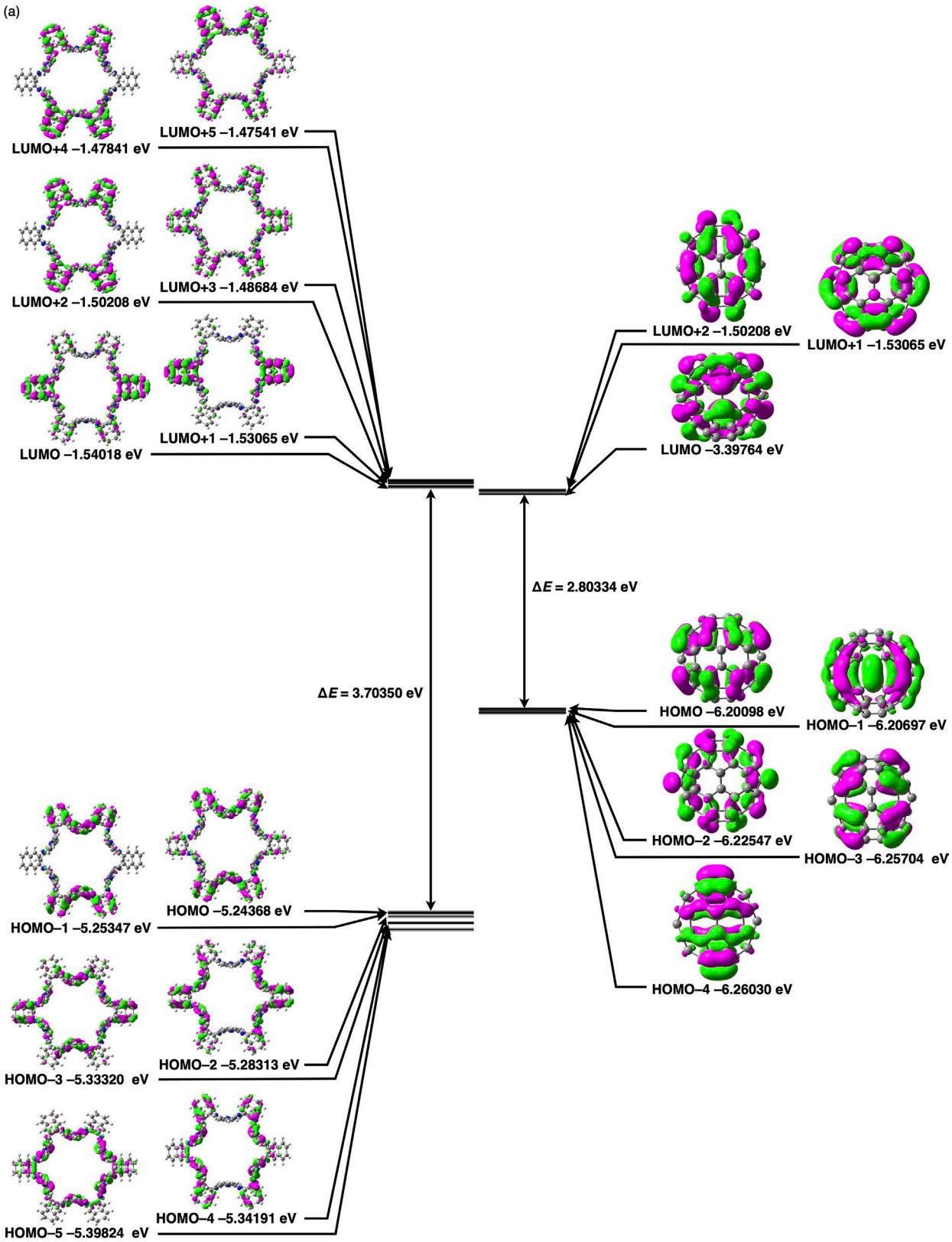

Fig. S23 Molecular orbitals (HOMO/LUMO) of (a) **2a**$_6$ (left) and C_{60} (right) and (b) **2a** (Forms A and B (left and middle, respectively)) and C_{60} (right) estimated at B3LYP/6-31G(d,p) for the crystal structure (Fig. S8,13). Energy levels of **2a**$_6$ and C_{60} suggest the possibility of electron transfer from **2a**$_6$ (donor) to C_{60} (acceptor).

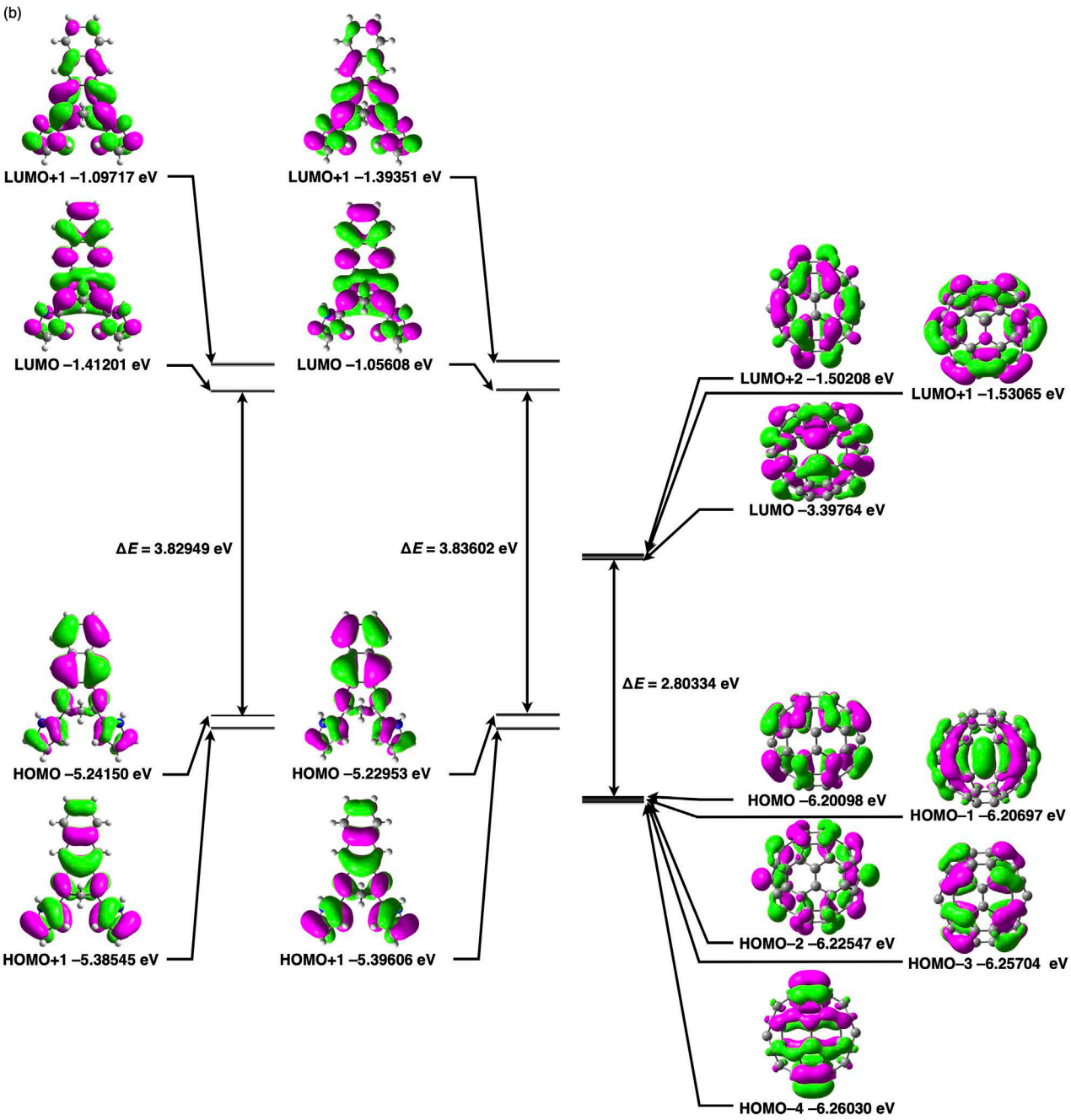

Fig. S23 (Continued)

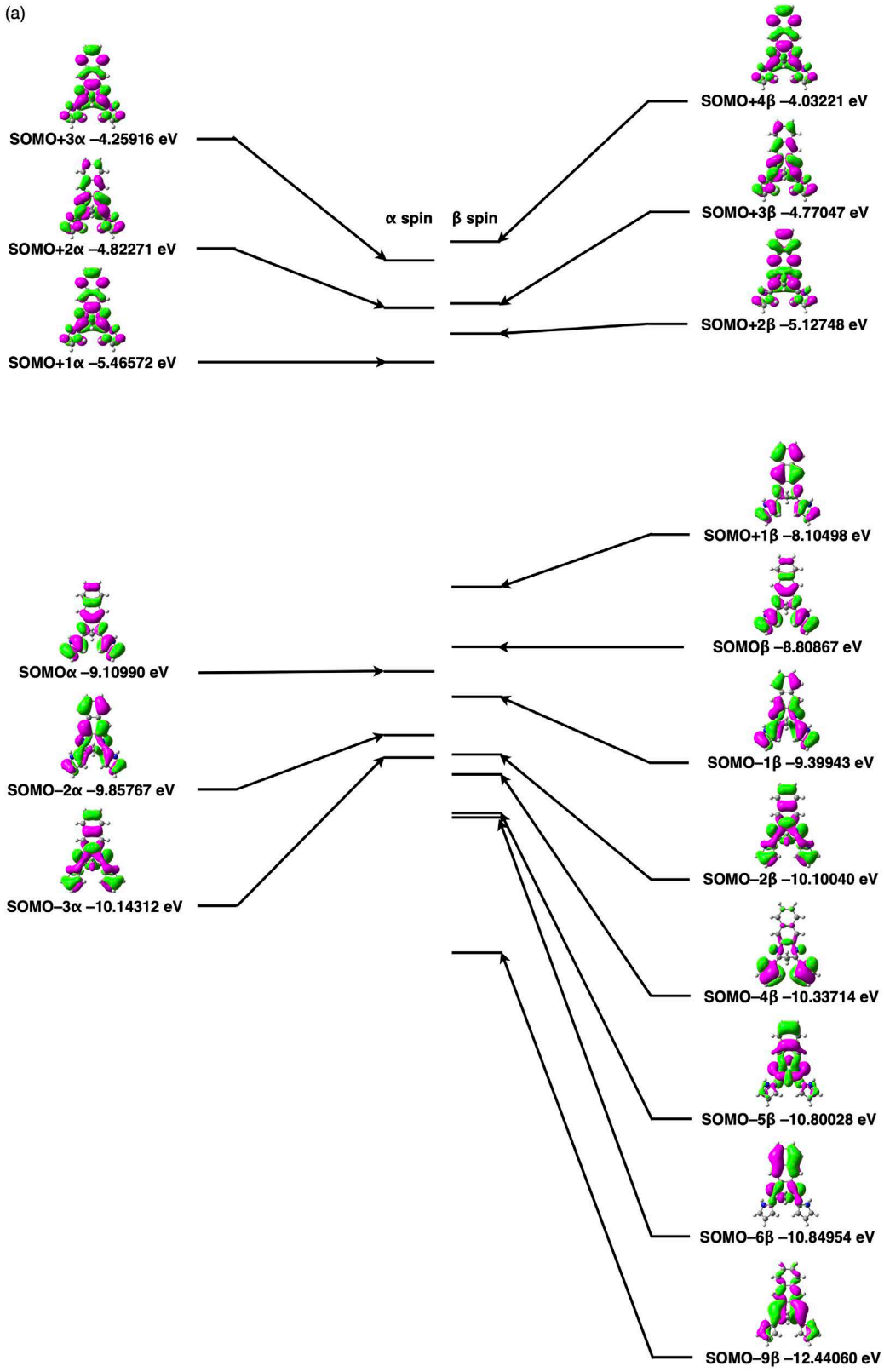

Fig. S24 Molecular orbitals of **2a** radical cation, which can be formed by photo-induced electron transfer, derived from the independent structures, (a) Form A and (b) Form B, in the crystal structure of $\mathbf{2a}_6 \cdot C_{60}$ (Fig. S8,13), estimated by single-point calculations at UB3LYP/6-31+G(d,p).

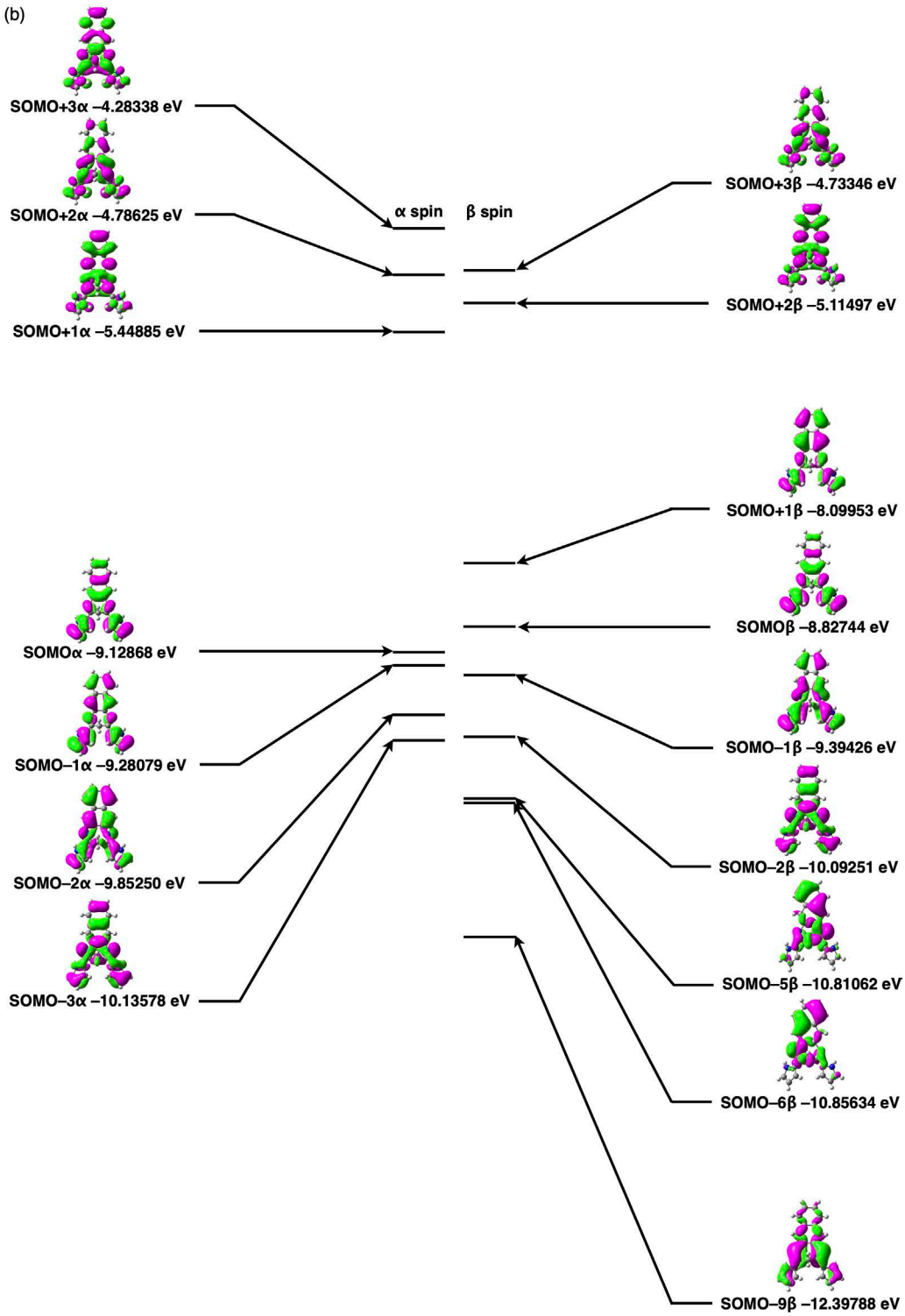

Fig. S24 (Continued)

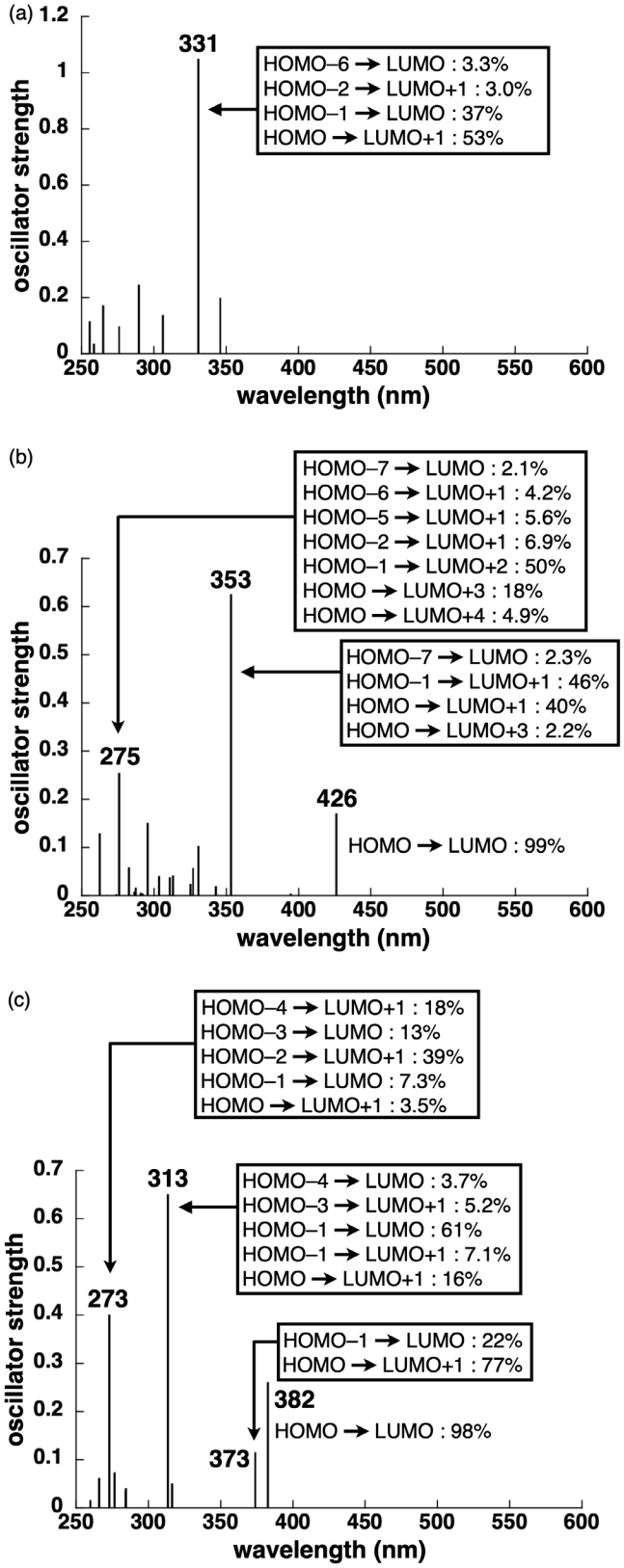

Fig. S25 TD-DFT-based UV/vis absorption stick spectra of (a) **2a**, (b) **2b**, and (c) **2c** with the transitions correlated with molecular orbitals (MOs) (Fig. S21) estimated at B3LYP/6-31G(d,p).

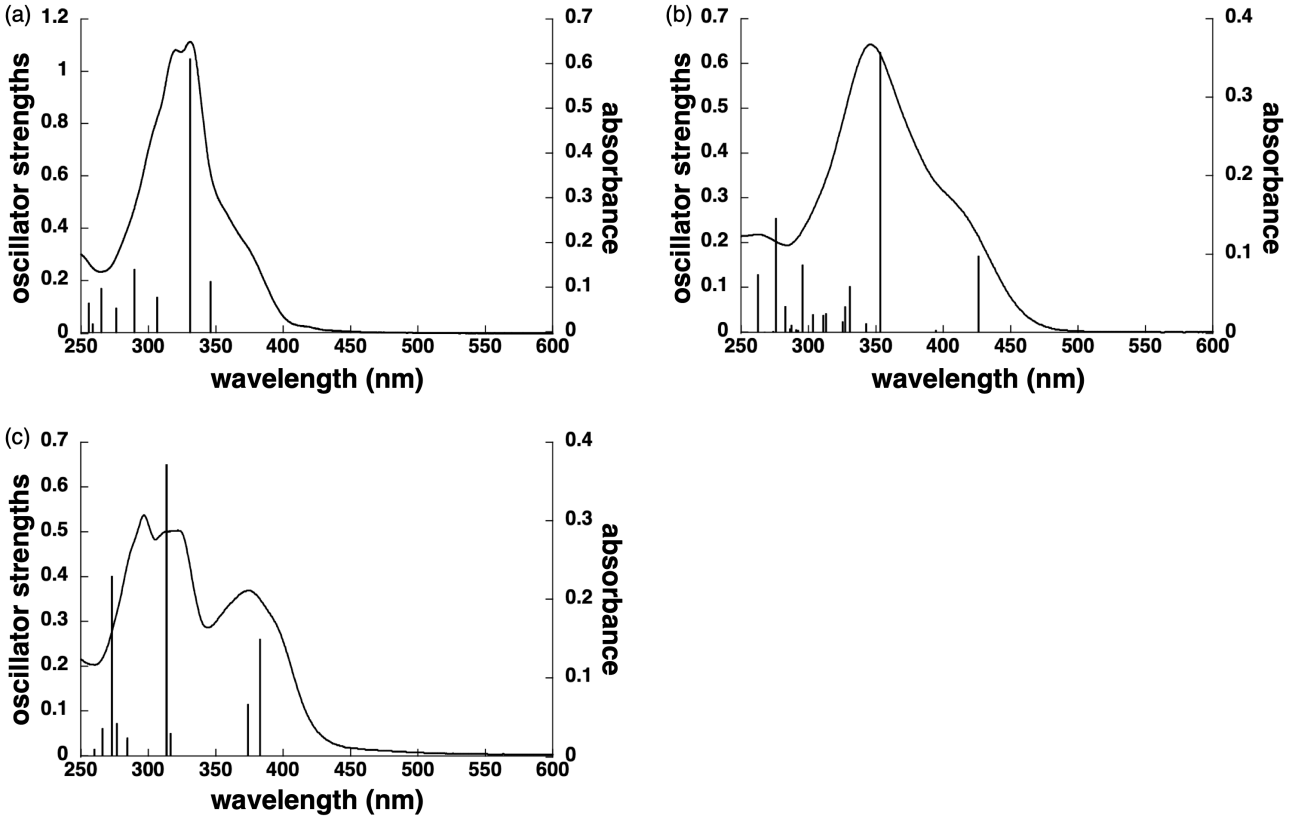

Fig. S26 Overlapped UV/vis absorption spectra (CH_2Cl_2, 1×10^{-5} M) (Fig. S4a) and TD-DFT-based UV/vis absorption stick spectra at B3LYP/6-31G(d,p) (Fig. S25) of (a) **2a**, (b) **2b**, and (c) **2c**.

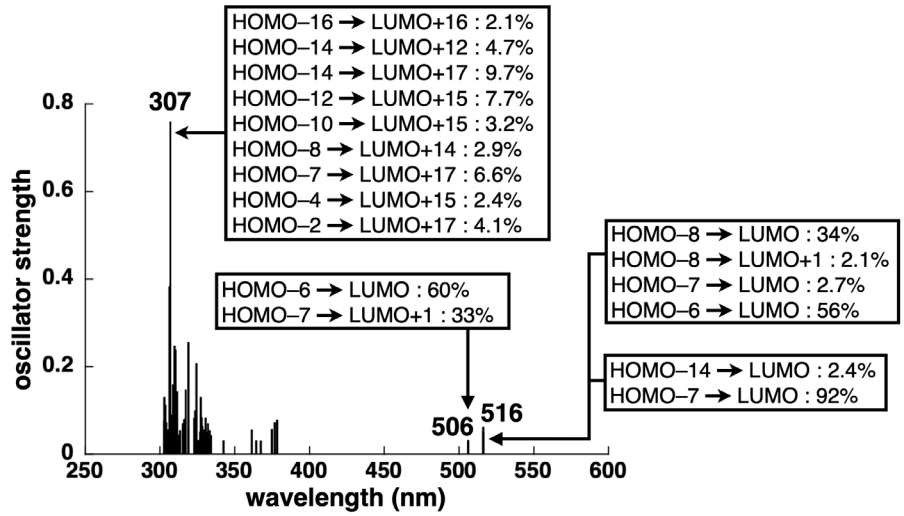

Fig. S27 TD-DFT-based UV/vis absorption stick spectrum of $\mathbf{2a}_6 \cdot C_{60}$ with the transitions correlated with MOs (Fig. S22) estimated at B3LYP/6-31G(d,p).

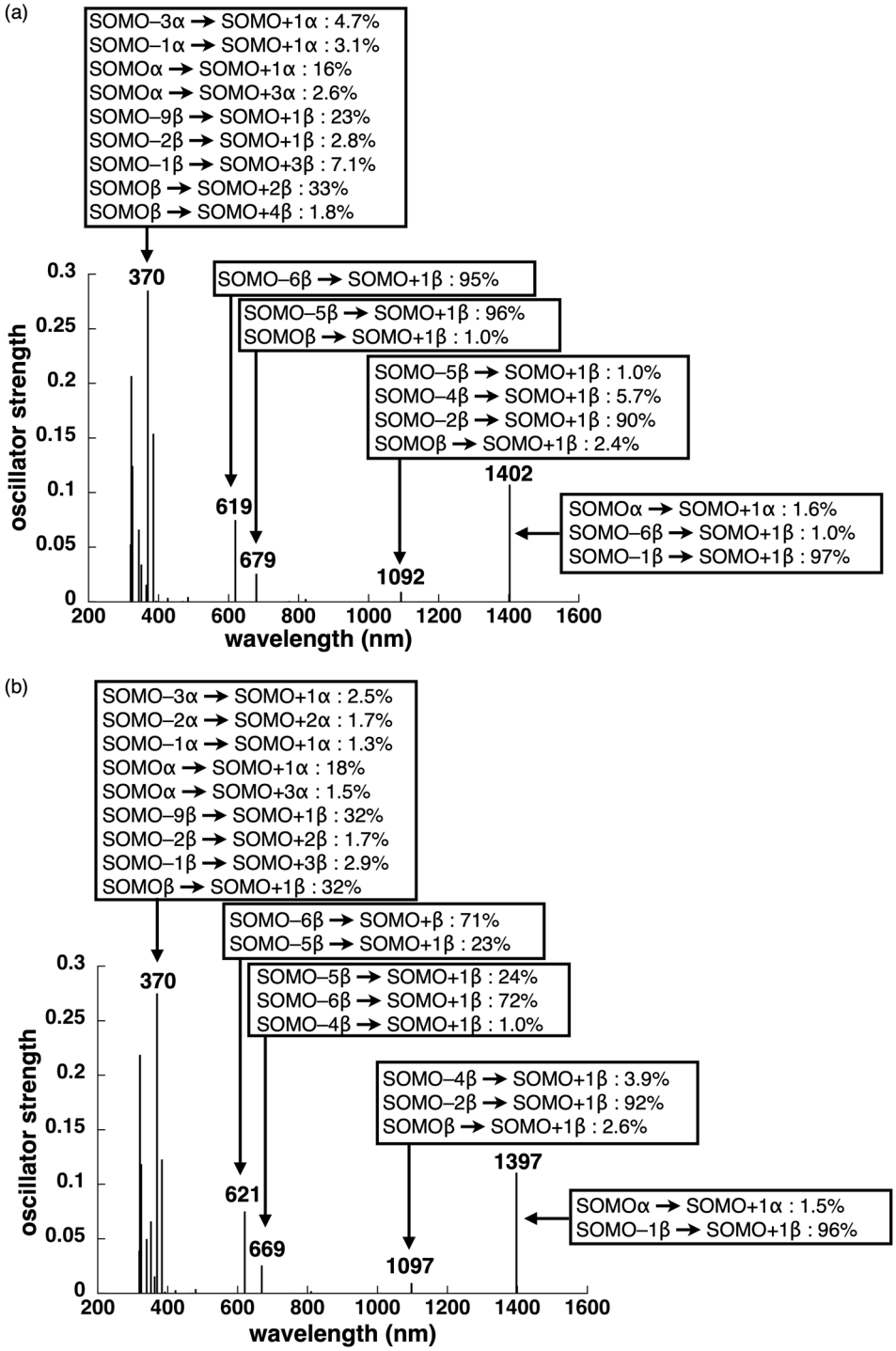

Fig. S28 TD-DFT-based UV/vis absorption stick spectra of **2a** radical cation derived from (a) Form A and (b) Form B in the crystal structure of **2a**$_6$·C_{60} with the transitions correlated with MOs (Fig. S24) estimated at UB3LYP/6-31+G(d,p).

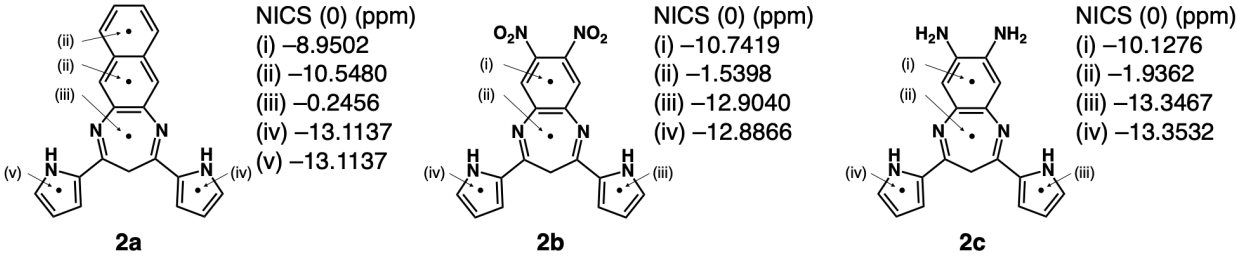

Fig. S29 Nucleus-independent chemical shifts (NICS) (ppm)[S3] of **2a**–**c** at B3LYP/6-31G(d,p). NICS values of the seven-membered diazepine ring indicate a weak aromaticity attributed to homoaromatic ring current of the diazepine units.

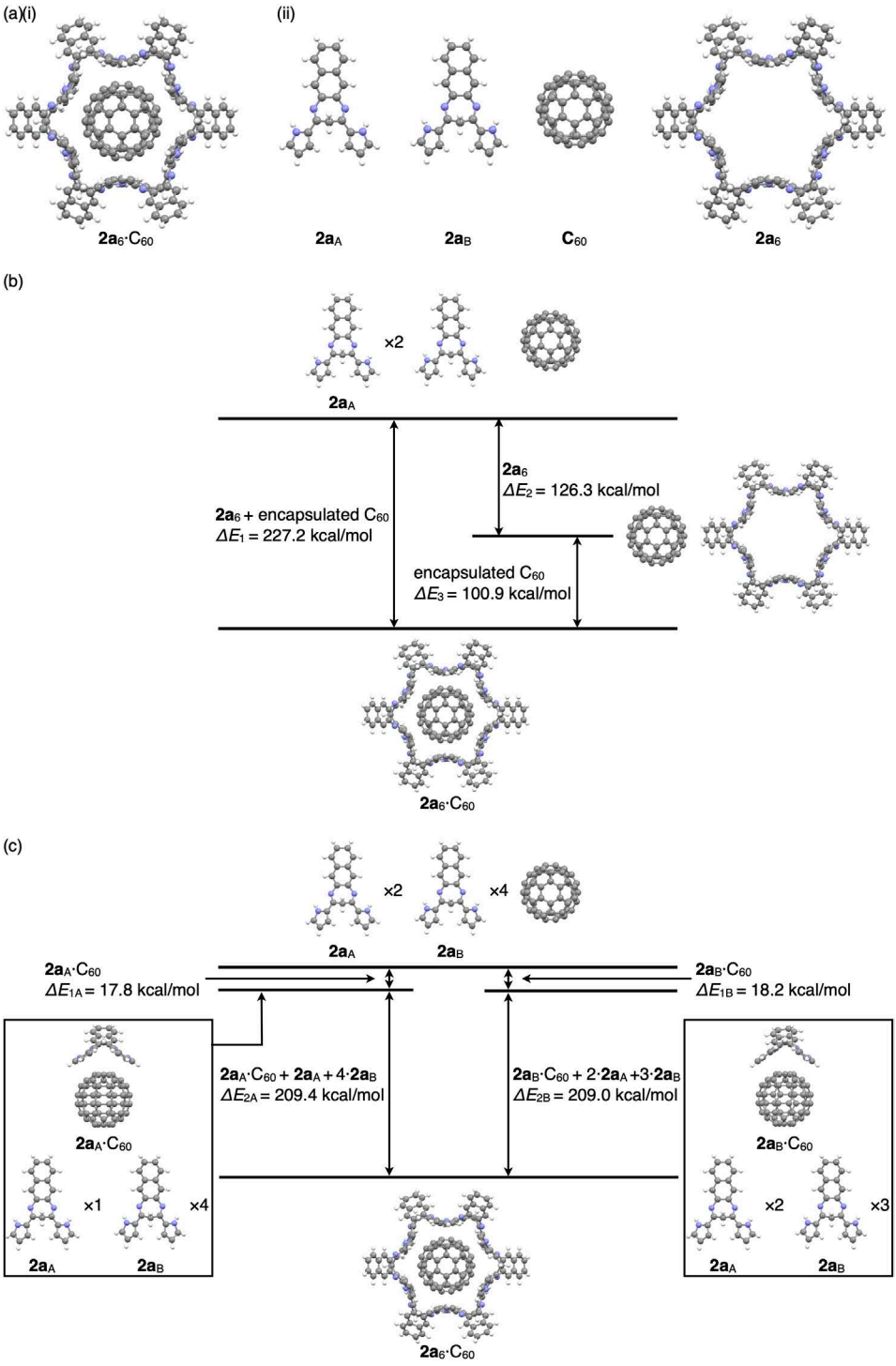

Fig. S30 (a) Crystal structure of (i) **2a**$_6$·C_{60} and (ii) the components of **2a**$_6$·C_{60}: **2a**$_A$ (Form A), **2a**$_B$ (Form B), C_{60}, and **2a**$_6$ (Fig. S8,13), (b) energy diagram for the solid-state assembling states, based on the hypothetical hydrogen-bonding hexamer **2a**$_6$, estimated at B3LYP-GD3BJ/6-31G(d,p), and (c) energy diagram for the solid-state assembling states, via the complexes **2a**·C_{60}, estimated at B3LYP-GD3BJ/6-31G(d,p). In (b), the stabilization energy for complementary hydrogen bonds between two **2a** molecules and that for the complexation of a **2a** molecule with C_{60} in **2a**$_6$·C_{60} were estimated to be 21.1 and 16.8 kcal/mol, respectively. On the other hand, in (c), the stabilization energies for the complexation of **2a** and C_{60} extracted from **2a**$_6$·C_{60} were 17.8 and 18.2 kcal/mol for **2a**$_A$ and **2a**$_B$, respectively, which are larger than that estimated from **2a**$_6$·C_{60} (16.8 kcal/mol). This energy difference can be derived from the polarization of C_{60}, which was supported by the electrostatic potential calculations. The complex **2a**·C_{60} exhibited highly polarized C_{60} because of the complexation at one side of C_{60}, whereas more symmetrical **2a**$_6$·C_{60} showed no such polarization, resulting in more favorable state in the isolated **2a**·C_{60} than the corresponding part in **2a**$_6$·C_{60}. Furthermore, as seen in (b) and (c), **2a**$_6$, **2a**·C_{60}, and **2a**$_6$·C_{60} are more stable than the components (**2a**$_A$ and **2a**$_B$ for **2a**$_6$ and **2a**·C_{60}; **2a**$_6$ and C_{60} for **2a**$_6$·C_{60}), but the formation of **2a**$_6$·C_{60} was not observed in solution state probably due to the entropy factor. The formation of **2a**·C_{60} will be discussed elsewhere.

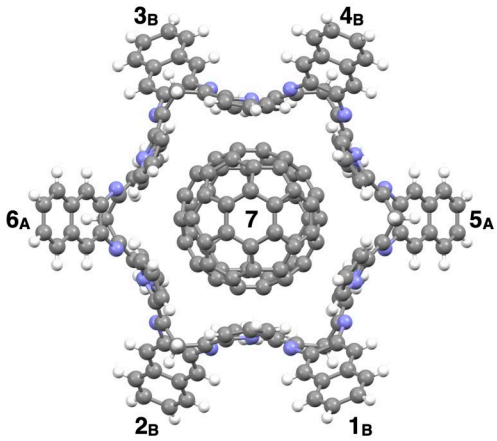

Fig. S31 Crystal structure of **2a**$_6$·C_{60} with the labels indicating the numbers of fragment and their Form (A or B) for **2a**. According to the EDA analysis (Table S2), total energies of –23.16 and –22.86 kcal/mol were observed for proximally located **2a** for Forms A/B and B/B, wherein electrostatic interaction energies (E_{es}) and dispersion interaction energies (E_{disp}) were –17.75 and –18.14 kcal/mol and –14.28 and –15.61 kcal/mol, respectively, as mainly contributed favorable interaction energies. E_{es} and E_{disp} can be derived from the complementary hydrogen bonds in the ring structure. On the other hand, total energies of –26.43 and –27.65 kcal/mol were observed for **2a** and C_{60} for Forms A and B, respectively, wherein E_{disp} were –29.95 and –33.00 kcal/mol as the energies of mainly contributed favorable interactions correlated with π–π stacking between pyrrole rings and C_{60}. Furthermore, electrostatic and charge-transfer interaction energies as smaller contributions to the interactions between **2a** and C_{60} were observed and can be ascribed to the proximally located electron-rich concave of **2a** and electron-deficient C_{60} as also supported by ESP and TD-DFT calculations (Fig. S20,22,23).

Table S2 Energies between each fragment in **2a**$_6$·C_{60} (Fig. S31) estimated by energy decomposition analysis (EDA)[S4] calculation based on a fragment molecular orbital (FMO) method (FMO2-MP2/cc-pVDZ level of theory).[S5–7]

fragments	total interaction energy (kcal/mol)	electrostatic interaction energy (E_{es}) (kcal/mol)	dispersion interaction energy (E_{disp}) (kcal/mol)	charge-transfer interaction energy (E_{ct}) (kcal/mol)	exchange repulsion interaction energy (E_{ex}) (kcal/mol)
2_B–1_B	–22.861	–18.135	–15.612	–4.202	15.089
3_B–1_B	–0.008	–0.008	0.000	0.000	0.000
3_B–2_B	0.239	1.041	–0.808	–0.132	0.138
4_B–1_B	0.239	1.041	–0.808	–0.132	0.138
4_B–2_B	–0.008	–0.008	0.000	0.000	0.000
4_B–3_B	–22.845	–18.124	–15.612	–4.202	15.093
5_A–1_B	–23.159	–17.747	–14.283	–3.754	12.625
5_A–2_B	0.156	1.004	–0.858	–0.161	0.170
5_A–3_B	0.154	1.002	–0.858	–0.161	0.171
5_A–4_B	–23.149	–17.731	–14.275	–3.752	12.608
6_A–1_B	0.156	1.003	–0.858	–0.161	0.171
6_A–2_B	–23.154	–17.737	–14.282	–3.753	12.618
6_A–3_B	–23.145	–17.721	–14.274	–3.751	12.601
6_A–4_B	0.154	1.001	–0.858	–0.161	0.171
6_A–5_A	0.016	0.016	0.000	0.000	0.000
7–1_B	–27.642	–5.256	–32.987	–5.374	15.975
7–2_B	–27.644	–5.256	–32.992	–5.376	15.980
7–3_B	–27.652	–5.260	–32.999	–5.379	15.986
7–4_B	–27.650	–5.260	–32.995	–5.377	15.981
7–5_A	–26.423	–3.853	–29.938	–4.623	11.990
7–6_A	–26.426	–3.857	–29.947	–4.627	12.004

Cartesian Coordination of 2a-1

-1028.9052434 hartree

C,-6.004609195,-0.7102283744,-0.0161463438
C,-4.8190871965,-1.4052058621,-0.0331779695
C,-3.5718915452,-0.7179577177,-0.0482290855
C,-3.5718913537,0.7179585853,-0.048229327
C,-4.8190868216,1.4052070675,-0.0331784442
C,-6.0046090057,0.7102299018,-0.016146588
H,-2.311746723,-2.4756113226,-0.1252595969
H,-6.9495780831,-1.2454603548,-0.0032042231
H,-4.8159419477,-2.4921004738,0.0342202637
C,-2.3350836731,-1.3905010048,-0.0831838178
C,-2.3350833021,1.390501531,-0.083184279
H,-4.8159412829,2.4921016779,-0.0342211048
H,-6.9495777509,1.2454621386,-0.003204645
C,-1.1126613655,0.7249761179,-0.0505260374
C,-1.1126615586,-0.7249759071,-0.0505258003
H,-2.3117460625,2.4756118286,-0.1252604175
N,0.0245320074,1.5279757372,-0.1378435729
N,0.0245315991,-1.5279758608,-0.1378430743
C,1.1504486165,1.2220138058,0.4228495046
C,1.150448289,-1.2220140511,0.4228499089
C,1.3171714959,0.0000000021,1.302798684
H,0.5160291683,0.0000002261,2.0526079653
H,2.272792235,-0.0000000421,1.8251883114
C,2.2844676181,2.091642861,0.1838821864
C,3.6002246621,2.1000686615,0.6454083291
N,2.1468372668,3.176223216,-0.6545435195
C,4.2497892215,3.2146071684,0.0660833971
H,4.0419510986,1.3832681047,1.3220770215
C,3.3201914301,3.8623312845,-0.7331328764
H,1.2664000581,3.3811551555,-1.1048495391
H,5.2775530982,3.5146891208,0.2113100392
H,3.4141937953,4.7490556786,-1.3425446002
C,2.2844670687,-2.0916434637,0.1838828398
C,3.6002241393,-2.1000694073,0.6454089037
N,2.146836 4365,-3.1762240338,-0.6545425418
C,4.2497883352,-3.2146084095,0.066084517
H,4.0419507796,-1.3832687257,1.3220773309
C,3.3201904377,-3.8623323981,-0.7331317365
H,1.2663991765,-3.3811558773,-1.1048485048
H,5.2775520939,-3.5146906672,0.2113113634
H,3.4141925796,-4.7490569856,-1.3425432131

Cartesian Coordination of 2a-2

-1028.8970496 hartree

C,3.474671644,4.3798391901,-1.2112470154
C,2.9412303265,3.8767191658,-0.0491047242
C,1.977034026,2.8291979628,-0.0838580159
C,1.5666108628,2.3054806594,-1.3568248086
C,2.1384338703,2.8535070686,-2.5408524585
C,3.0686051565,3.8624427605,-2.4705173839
H,1.6641140981,2.6990039609,2.0538591759
H,4.2103519567,5.1778621986,-1.1723819939
H,3.2488926972,4.2708411855,0.9159964954
C,1.3951532744,2.2953526167,1.0819702546
C,0.5950332328,1.2870879705,-1.3858620751
H,1.8246796589,2.4573174098,-3.5030150108
H,3.4983596429,4.2710173844,-3.3804768585
C,0.0671609386,0.7148462152,-0.2308594494
C,0.4918247913,1.2367128866,1.0552949639
H,0.2308354486,0.9134980903,-2.3383464441
N,-0.9460882723,-0.2236097404,-0.4117195874
N,-0.0111167797,0.8316674605,2.2951998058
C,-1.12721958,-1.2162186685,0.3930584611
C,-0.3342779154,-0.3962100684,2.5427218526
C,-0.1528378934,-1.5003729581,1.5286639829
H,0.864330333,-1.4472326643,1.1219255833
H,-0.2883422133,-2.4928946124,1.9590161004
C,-2.2883918799,-2.0696633347,0.2072834716
C,-3.1323949074,-2.2029084435,-0.8898813874
N,-2.7472258284,-2.9469281244,1.1787625443
C,-4.1158856603,-3.1649065758,-0.5656805116
H,-3.0112428936,-1.6672666186,-1.8193463686
C,-3.8668218042,-3.5906871031,0.7272785914
H,-2.4510425492,-2.9325336348,2.143509796
H,-4.9138609305,-3.5177072133,-1.2034476589
H,-4.3949007498,-4.2946628663,1.353238258
C,-0.9368009575,-0.705146511,3.8269964861
C,-1.2591336155,-1.9038180244,4.4654241053
N,-1.2960246139,0.3111685116,4.6806164152
C,-1.8219581862,-1.5804922139,5.7241520138
H,-1.0592697615,-2.8995944507,4.0933588252
C,-1.8299929935,-0.1991868172,5.8263907322
H,-1.1442973595,1.2795105904,4.435995238
H,-2.1746664259,-2.2728017513,6.4749193237
H,-2.1764721276,0.4445848369,6.6211677757

Cartesian Coordination of 2a-3

-1028.8849167 hartree

C,5.5592649496,-1.1316908956,-1.339586471
C,4.7534171704,-1.4047002704,-0.2608799012
C,3.5730050314,-0.6436669366,-0.0216453499
C,3.2387382032,0.4201030968,-0.9279655871
C,4.0994747123,0.6764047985,-2.0339582739
C,5.2286862199,-0.079657859,-2.2359069176
H,2.9873206763,-1.6452632026,1.8061060753
H,6.4561167741,-1.7195389265,-1.5121048782
H,5.0046423325,-2.2072738522,0.4276271364
C,2.7314835941,-0.8776174504,1.0817197115
C,2.0839310072,1.183152506,-0.6740333715
H,3.845035473,1.4830565175,-2.7164932949
H,5.8766245596,0.1246358474,-3.0833212748
C,1.2129390109,0.9043314058,0.3775031073
C,1.550149785,-0.1688074349,1.2918054641
H,1.8351059287,2.021542526,-1.317971623
N,0.1372364489,1.7753313719,0.5240544438
N,0.8478640389,-0.4861683387,2.4508270449
C,-1.0079725571,1.4134497753,0.9986794037
C,-0.4373214834,-0.4025889714,2.5459242179
C,-1.2962760582,-0.042373306,1.3408957871
H,-0.9831265339,-0.665214063,0.4943574449
H,-2.3589136545,-0.2350071461,1.506716196
C,-2.0108526596,2.4427007187,1.2214917385
C,-1.8701794032,3.8265338393,1.1800985762
N,-3.3406586309,2.1896045917,1.5234415998
C,-3.1300766926,4.4038911228,1.451912318
H,-0.9377953559,4.3330040642,0.9822914626

C,-4.0242892811,3.3673808177,1.6537524171
H,-3.7701240333,1.2806207786,1.5504308928
H,-3.364347995,5.4575402745,1.5043422726
H,-5.0801796599,3.377651573,1.8801642891
C,-1.0425387124,-0.6388594994,3.8469467713
C,-0.4283088698,-0.7620718376,5.0895395785
N,-2.4042014886,-0.7905745991,4.0625211248
C,-1.4327519497,-0.9976714799,6.0539835795
H,0.6356539755,-0.6743376959,5.2484909506
C,-2.646420255,-1.0175466003,5.3896618082
H,-3.1081879436,-0.825923206,3.3451829387
H,-1.294043527,-1.1306319678,7.1173917495
H,-3.6509349283,-1.1707737796,5.755372102

Cartesian Coordination of 2b-1

-1284.2429229 hartree

C,-1.5961377008,1.2144400028,-0.4514328251
C,-1.7645985831,-0.0075132613,-1.3308618646
C,-1.5970891044,-1.2173530438,-0.4343283636
C,0.6639379312,0.7164549314,0.0014637685
C,0.6633899464,-0.7157371585,0.0147434734
H,-2.722042127,-0.0109407938,-1.848968826
C,1.9075621099,1.3854115373,0.0517758998
H,1.9114067416,2.4667907052,0.1069648316
C,1.9071889588,-1.3860008026,0.0501546478
H,1.9117594676,-2.4689135626,0.0594067188
C,3.1057548558,0.7037705337,0.044209854
C,3.1049517083,-0.7044481711,0.0307004328
N,4.3314637516,-1.4980051641,-0.1342933454
O,5.1898212752,-1.0475638983,-0.8866054493
O,4.3817430725,-2.5811146891,0.4448723485
N,4.332029884,1.4931450567,0.222955427
O,5.2043553184,1.0171213647,0.9431698142
O,4.3712241985,2.598014407,-0.315298336
C,-2.7279348984,2.0666769635,-0.1829496255
C,-4.0527369227,2.0627533893,-0.625456936
N,-2.5931921643,3.1445874813,0.6674675832
C,-4.7074982699,3.158495157,-0.0244815583
H,-4.4942652272,1.3499686024,-1.3063184718
C,-3.7734036266,3.8105875248,0.7691938058
H,-1.7119525176,3.366956565,1.1076861546
H,-5.7406345362,3.4472066066,-0.1515024893
H,-3.8714251289,4.6907525705,1.3873983533
C,-2.7296055519,-2.0636266633,-0.1519114302
C,-4.054552779,-2.0657807107,-0.5943564726
N,-2.5957680477,-3.127514087,0.7162853419
C,-4.7100506807,-3.1510553754,0.0242607639
H,-4.4955425103,-1.3635673839,-1.2864759257
C,-3.7762782303,-3.7910252003,0.8283390772
H,-1.7143910672,-3.3439424533,1.1594020574
H,-5.7434667975,-3.4408899675,-0.0978217378
H,-3.875138687,-4.6607056612,1.4610865653
H,-0.9653750965,-0.0130027646,-2.0817386434
N,-0.4535859965,1.5266826922,0.0832629839
N,-0.4542822181,-1.524286449,0.1033396076

Cartesian Coordination of 2b-2

-1284.2345228 hartree

C,1.550347983,1.2197442286,0.440945065
C,0.608995012,1.5066083735,1.6024208424
C,0.8492871712,0.4113195522,2.6148695265
C,0.361494899,-0.7278748165,-0.1197883307
C,0.0016321975,-1.2421050976,1.1690836761
H,0.7466422859,2.5037490558,2.0201660113
C,-0.1877843785,-1.3515077927,-1.2649425869
H,0.1291806592,-1.0074227405,-2.2415178796
C,-0.8859562523,-2.3384996445,1.2319983987
H,-1.155970733,-2.7325249226,2.2039091836
C,-1.0912083032,-2.3867408727,-1.168197845
C,-1.4531467267,-2.8832090317,0.0996066197
N,-2.5165395324,-3.8791642914,0.2873001713
O,-3.4780887804,-3.8193941398,-0.4731656354
O,-2.3940015368,-4.6619455123,1.2275469911
N,-1.5036899644,-3.039109044,-2.420195372
O,-1.5698663346,-4.2642528031,-2.4160267634
O,-1.6947377256,-2.3126630565,-3.3929220829
C,2.7102690366,2.052236261,0.2160927559
C,3.5548567006,2.1175747715,-0.8904416169
N,3.1730578123,2.986553476,1.1325478127
C,4.5377325339,3.0937287561,-0.6270966494
H,3.4303814019,1.5290006331,-1.7868408746
C,4.290496845,3.5973152394,0.6400756888
H,2.8778432093,3.0387463489,2.0958329529
H,5.3353838578,3.406215025,-1.2854498212
H,4.8229257116,4.3360176633,1.2207182538
C,1.5035412034,0.7297419221,3.8641726997
C,1.8335759743,1.9388502094,4.4826008733
N,1.9166195381,-0.2760649621,4.7086167362
C,2.4546275431,1.6337864796,5.7146580043
H,1.6000334756,2.9291176226,4.1155046374
C,2.4896925521,0.2516198733,5.8243102584
H,1.7710309628,-1.2506992178,4.4861552495
H,2.8268307755,2.3359584528,6.446274816
H,2.8794009417,-0.3799291291,6.6087991465
H,-0.4205898483,1.4363948825,1.2328743813
N,1.3301474681,0.2237768226,-0.3584582118
N,0.5189375347,-0.8229085346,2.3850420068

Cartesian Coordination of 2b-3

-1284.2241571 hartree

C,1.4357706211,-1.356867142,1.0721704303
C,1.6758881004,0.1133204617,1.3612793393
C,0.8814940334,0.4162284632,2.6233933875
C,-0.8287259533,-0.9498020988,0.5890589449
C,-1.1468482716,0.1287233849,1.4789244661
H,2.7287974034,0.3763195364,1.4723906958
C,-1.7778582288,-1.3096323076,-0.3944338319
H,-1.5724983492,-2.1689911662,-1.0204055034
C,-2.3783120364,0.8034297833,1.3026032882
H,-2.622880525,1.6183768017,1.9727371277
C,-2.9484736217,-0.6042533729,-0.5701462421
C,-3.2447733677,0.4777942414,0.2833217895
N,-4.3901268148,1.3733756341,0.0585294112
O,-4.6576950316,1.6505732339,-1.1065528828
O,-4.9530398802,1.826385035,1.0521447482
N,-3.9151535457,-1.1288392367,-1.5435510033
O,-5.1030690745,-1.071524589,-1.2397199374
O,-3.4613304399,-1.636505904,-2.5674727439
C,2.4937924452,-2.3206833861,1.3048057768
C,2.4176202701,-3.6921290605,1.508593719

N,3.8397330983,-1.9702863852,1.411434887
C,3.730244114,-4.1790289529,1.7099097162
H,1.4951370447,-4.2527062386,1.5344129488
C,4.5894795453,-3.1014260285,1.6192059117
H,4.2293448458,-1.1089383111,1.0589533007
H,4.0185611746,-5.200419617,1.9124857729
H,5.6662085667,-3.0497872544,1.6865281077
C,1.561140132,0.6154373002,3.8841751726
C,1.0731314642,1.1276299664,5.0838298715
N,2.9019076472,0.3166418284,4.0880090863
C,2.1306388543,1.1249265319,6.0175984769
H,0.0636033409,1.4816940319,5.228695976
C,3.2415863504,0.5958295669,5.3818849838
H,3.4655904883,-0.2424176524,3.4650679366
H,2.0951555394,1.4744938684,7.0392931585
H,4.2367606707,0.3974962841,5.7515020227
H,1.2650866751,0.7149559174,0.5427561232
N,0.276713334,-1.7784920164,0.6754953575
N,-0.4115785487,0.491280269,2.5868052296

Cartesian Coordination of 2c-1

-985.9773906 hartree
C,1.53380785,-0.71358753,-0.00399208
C,1.53410384,0.71474616,0.00362993
C,-0.73235551,1.21543291,0.4326273
C,-0.73251377,-1.21764117,0.42353918
C,-0.90677784,-0.00430601,1.30985523
H,-0.10391271,-0.00701004,2.05911587
H,-1.86571618,-0.00619504,1.82693358
C,-1.86715826,-2.07527835,0.14129065
C,-3.19168708,-2.08623835,0.57480577
N,-1.71738404,-3.14308994,-0.71600414
C,-3.83449514,-3.1872236,-0.03993165
H,-3.64358856,-1.38018231,1.25607866
C,-2.89246588,-3.82356769,-0.83226953
H,-0.82801297,-3.34225697,-1.15068707
H,-4.86658592,-3.48473721,0.07831276
H,-2.9771599,-4.69785804,-1.46072461
C,-1.86727388,2.07437274,0.15522572
C,-3.1927244,2.08023896,0.58594471
N,-1.71686944,3.14947549,-0.69274742
C,-3.83555394,3.18541593,-0.02121799
H,-3.64538533,1.3677778,1.25998647
C,-2.89244112,3.82970712,-0.80576872
H,-0.82657752,3.35367625,-1.12309021
H,-4.86831347,3.48059354,0.09703822
H,-2.9766871,4.70932679,-1.42680318
C,2.77901069,-1.38203503,-0.03863335
H,2.75660337,-2.46820789,-0.05962238
C,2.77897244,1.38196788,-0.05570998
H,2.75572432,2.46686518,-0.11188604
C,3.98953328,-0.71114386,-0.01451184
C,3.98961091,0.71134078,-0.042379
N,5.23693961,-1.36371901,-0.04279709
H,5.89698891,-0.95312846,0.6114414
H,5.1650729,-2.36162728,0.11449526
N,5.23563254,1.36557516,-0.0226508
H,5.1640962,2.35890822,-0.20723748
H,5.90131091,0.93685672,-0.6593784
N,0.41015376,1.52808921,-0.09485459
N,0.40932612,-1.52576039,-0.10794579

Cartesian Coordination of 2c-2

-985.9696727 hartree
C,0.4810108295,0.7353050738,-0.1272194226
C,0.8625417696,1.2286737654,1.1601824635
C,0.0131536816,-0.4310909287,2.5976395062
C,-0.7087789055,-1.2166601637,0.4224998989
C,0.2414673776,-1.5116666562,1.571983148
H,1.2668059458,-1.4240242431,1.1898131689
H,0.1126785527,-2.5155165859,1.9783213215
C,-1.8692643758,-2.0646983454,0.2011516694
C,-2.6921038848,-2.1834532219,-0.9129740424
N,-2.3459399119,-2.9543120506,1.152005597
C,-3.6816891569,-3.1508353916,-0.6198600575
H,-2.5546879032,-1.6349818533,-1.8326431316
C,-3.4576341548,-3.5931187149,0.6713913954
H,-2.0703994881,-2.9474823616,2.1231466804
H,-4.4671496127,-3.4953917855,-1.2775856031
H,-3.9968296944,-4.3049805248,1.2786512301
C,-0.6402484207,-0.7618215372,3.852374563
C,-0.9700438257,-1.9710918735,4.465683044
N,-1.0499446342,0.2399479661,4.6999133349
C,-1.5881013836,-1.6685339523,5.7049624333
H,-0.7387880119,-2.9596829757,4.0924350357
C,-1.6211887227,-0.2895421568,5.8204836039
H,-0.9005720001,1.2121650084,4.4704838249
H,-1.9605225458,-2.3739234995,6.4338831238
H,-2.0085529132,0.3414372567,6.6065790912
C,1.0248731194,1.3651115607,-1.270454772
H,0.7075511499,0.9889207882,-2.2389985293
C,1.7259891367,2.3466559491,1.2193436067
H,1.9510359801,2.7461765849,2.2044661983
C,1.939738672,2.400341377,-1.189283474
C,2.2836654083,2.9203490552,0.0906707584
N,2.4937613584,3.0318706564,-2.3177743334
H,3.4890321124,3.2045952435,-2.2106496456
H,2.3141002615,2.5331827904,-3.1806124304
N,3.2084907146,3.9806182396,0.1378070602
H,3.2819267756,4.400537026,1.0566385713
H,3.0066433011,4.6928040132,-0.5582829698
N,0.3464607412,0.8029524107,2.3816558209
N,-0.5059961024,-0.2120587131,-0.3656732682

Cartesian Coordination of 2c-3

-985.9594293 hartree
C,1.6566352586,0.9255319183,0.54951854
C,1.9813770721,-0.1545911979,1.4308863554
C,-0.0271962184,-0.4345713803,2.6147948943
C,-0.5985105615,1.3474819849,1.07180043
C,-0.8371029535,-0.1187054311,1.3694250298
H,-0.4300765674,-0.715541099,0.5431402978
H,-1.8894898112,-0.3832268719,1.491884219
C,-1.654470448,2.3203482261,1.3158517125
C,-1.5801696489,3.6938307188,1.4924572692
N,-2.9963153424,1.9700210937,1.4511601623
C,-2.8938382761,4.1821993377,1.7045190293
H,-0.6585682565,4.2561991223,1.4916041441
C,-3.7509793805,3.1024427346,1.6522031615
H,-3.3837346892,1.0928830071,1.1389395035

H,-3.1815418699,5.2069128359,1.8926066219
H,-4.8252182461,3.0452451235,1.7480313216
C,-0.7005838008,-0.6514270264,3.8862115262
C,-0.2329958703,-1.2316215627,5.058943411
N,-2.0201011793,-0.2891840854,4.1132441732
C,-1.2847606649,-1.2062231749,6.005412049
H,0.7579567615,-1.6418922708,5.1820092857
C,-2.369265191,-0.5970136723,5.4022053098
H,-2.5513294761,0.3254237211,3.5142387736
H,-1.259456149,-1.595034113,7.0135928456
H,-3.3508358436,-0.3600020072,5.7850736227
C,2.591591877,1.2730532661,-0.4540611744
H,2.3351476314,2.1101022476,-1.0974653882
C,3.2283366423,-0.8007170063,1.2642932408
H,3.4850341299,-1.5709694509,1.9861710241
C,3.7689901792,0.5750549877,-0.6520826464
C,4.1045650646,-0.4812988891,0.2425969054
N,4.7062312197,0.9039795307,-1.6505123624
H,5.0526255084,0.0815204424,-2.1360849119
H,4.3527170986,1.5795221232,-2.3171551304
N,5.3125266783,-1.1658264804,0.0198105173
H,5.5691634404,-1.7767007363,0.7858512395
H,6.0757616142,-0.5314308429,-0.1974632247
N,1.2625538464,-0.5085031274,2.5640812935
N,0.5529567918,1.7647027743,0.6534061279

Cartesian Coordination of 2c´-1

-1518.261343 hartree

C,-4.2200273577,2.4990725694,-0.0462254116
C,-4.3425148964,1.0710543803,0.0562829828
C,-2.1684814262,0.4274184454,0.7175561094
C,-1.9605064382,2.8522556792,0.5435406295
C,-1.9569273788,1.6944074139,1.5195164038
H,-2.8059047506,1.8163761515,2.2043408518
H,-1.0418767402,1.658247402,2.1092786452
C,-0.7415476253,3.6008681193,0.3122644109
C,0.5408711013,3.5365912535,0.8554630051
N,-0.7340814045,4.621223415,-0.6134494545
C,1.3189293577,4.5424059322,0.2360690901
H,0.877578814,2.8422022752,1.6112902374
C,0.4979962129,5.198855793,-0.667829973
H,-1.5664908609,4.8630455345,-1.1316832198
H,2.3592441145,4.7660105777,0.4238947499
H,0.7046160588,6.0227420906,-1.3349338172
C,-1.0969217484,-0.5420633057,0.6096905377
C,0.1843201184,-0.6196728509,1.1539237535
N,-1.2737075004,-1.6697526617,-0.1617947465
C,0.7730347329,-1.8204120345,0.693129715
H,0.6429792867,0.1076982787,1.8076723724
C,-0.1581149122,-2.4496393035,-0.1186110683
H,-2.1412317187,-1.8379759183,-0.6507247457
H,1.7625429641,-2.1882310198,0.923597566
H,-0.1022176574,-3.3827921241,-0.6595447058
C,-5.3911696874,3.249875709,-0.2056360296
H,-5.2987090061,4.3278365043,-0.2830119255
C,-5.6257813709,0.5146227127,-0.0093012882
H,-5.7182404239,-0.5633381359,0.0680756006
C,-6.6744370668,2.6934455348,-0.2712163449
C,-6.7969229907,1.2654253181,-0.168718697
C,-8.8484874012,3.3371001726,-0.9325083485
C,-9.0564731867,0.9122610538,-0.758457741
C,-9.0600484836,2.0700986602,-1.7344453067
H,-9.9751008658,2.106253185,-2.3242045458
H,-8.2110743348,1.9481239349,-2.4192736365
C,-9.9200808182,4.306560222,-0.824594085
C,-11.2014152449,4.3840558757,-1.3686345939
N,-9.7432821068,5.4342843431,-0.0531552944
C,-11.7901499267,5.5847810021,-0.9078105495
H,-11.6601066412,3.6566305866,-2.0222975155
C,-10.8589384492,6.2140975769,-0.0962027483
H,-8.875729874,5.6025158417,0.4357306066
H,-12.7797085159,5.9525363207,-1.1381596478
H,-10.9148293817,7.1472797461,0.4446792495
C,-10.2754299031,0.1636020531,-0.5272319375
C,-11.5578677905,0.2279250087,-1.0703887239
N,-10.2829115816,-0.8567719803,0.398466853
C,-12.3358890657,-0.7780192519,-0.4511414059
H,-11.8945752589,0.9223586931,-1.8261733363
C,-11.5149928622,-1.4344142739,0.4528366161
H,-9.4505495761,-1.0984556919,0.9168496363
H,-13.3761636876,-1.0017192474,-0.6390719788
H,-11.7216153828,-2.2583427702,1.1198861102
N,-7.7336316868,3.5957254611,-0.3253660835
N,-7.9942521326,0.5572180852,-0.1072719306
N,-3.283334648,0.1687746526,0.1104346634
N ,-3.022705983,3.2072810942,-0.107674559

Cartesian Coordination of 2c´-2

-1518.2617924 hartree

C,1.2355468139,-0.7187106551,-0.035891494
C,-0.000000284,-1.3744482459,-0.1006451685
C,-1.2355481705,-0.7187092606,-0.0359203519
C,-1.2355473752,0.718709364,-0.0359258934
C,0.0000012471,1.3744464669,-0.1006557526
C,1.2355476149,0.7187079936,-0.0358970355
H,-0.000000021,-2.4563375549,-0.1774002707
H,0.0000027379,2.4563351863,-0.1774191738
C,-3.495455606,-1.2206972739,0.4265972579
C,-3.4954543026,1.220703319,0.4265877358
C,3.4954445312,1.2206992787,0.4266686242
C,3.4954432019,-1.220700864,0.4266778199
C,3.6627164595,0.0000024287,1.3072368018
C,-3.6627480825,0.0000065327,1.3071519729
N,-2.3638952614,1.5294326616,-0.1238717537
N,-2.3638969275,-1.5294320499,-0.1238599265
N,2.3638966853,-1.5294345557,-0.1238051061
N,2.3638983923,1.5294299903,-0.1238167713
H,-2.8594791468,0.0000090647,2.0550592454
H,-4.6183668897,0.0000091151,1.8298611103
H,2.8594306099,0.0000056783,2.0551258966
H,4.6183234054,0.0000038362,1.8299676406
C,-4.6301702935,2.085887978,0.1747348563
C,-5.949248847,2.0931520478,0.6262836634
N,-4.4887618289,3.1671368383,-0.6672242294
C,-6.5969120188,3.2044040962,0.0377964919
H,-6.3942859081,1.3776377135,1.3021482895
C,-5.6629364459,3.8511964464,-0.7567093471
H,-3.604507769,3.3730682951,-1.1095170161
H,-7.6264465898,3.5027031685,0.17416544
H,-5.7539416373,4.7357883331,-1.3696539095

C,-4.6301725591,-2.0858825763,0.174750901
C,-5.9492508221,-2.0931423894,0.6263006402
N,-4.4887655102,-3.1671375108,-0.6672006055
C,-6.596915176,-3.2043982908,0.0378220623
H,-6.3942869031,-1.3776229148,1.3021604721
C,-5.6629406037,-3.8511970826,-0.7566797246
H,-3.6045117448,-3.3730732672,-1.1094919713
H,-7.6264498803,-3.502695602,0.1741938551
H,-5.7539469102,-4.7357931988,-1.3696180145
C,4.6301676262,2.0858819362,0.1748408269
C,5.9492352994,2.0931454921,0.6264215172
N,4.4887808137,3.1671289871,-0.6671241784
C,6.5969135765,3.2043962562,0.0379485112
H,6.3942551698,1.3776319862,1.3022983609
C,5.6629578109,3.8511881576,-0.7565809524
H,3.6045371489,3.3730611054,-1.1094374388
H,7.626445097,3.5026946954,0.1743418421
H,5.7539787673,4.7357788474,-1.3695249181
C,4.6301652697,-2.0858868284,0.1748566781
C,5.9492331303,-2.0931480657,0.6264368431
N,4.4887769256,-3.1671406488,-0.6670993678
C,6.5969100809,-3.2044041178,0.0379723591
H,6.3942540307,-1.3776295242,1.3023076706
C,5.6629533212,-3.8512014723,-0.756551493
H,3.6045330176,-3.3730750408,-1.1094110818
H,7.6264413813,-3.5027024537,0.1743675845
H,5.7539730984,-4.7357972122,-1.3694883446

[S3] P. v. R. Schleyer, C. Maerker, A. Dransfeld, H. Jiao and N. J. R. van Eikema Hommes, *J. Am. Chem. Soc.*, 1996, **118**, 6317–6318.

[S4] M. J. S. Phipps, T. Fox, C. S. Tautermann and C.-K. Skylaris, *Chem. Soc. Rev.*, 2015, **44**, 3177–3211.

[S5] Articles for *GAMESS*: (a) M. W. Schmidt, K. K., Baldridge, J. A. Boatz, S. T. Elbert, M. S. Gordon, J. H. Jensen, S. Koseki, N. Matsunaga, K. A. Nguyen, S. J. Su, T. L. Windus, M. Dupuis and J. A. Montgomery, *J. Comput. Chem.*, 1993, **14**, 1347−1363; (b) M. S. Gordon and M. W. Schmidt, in *Theory and Applications of Computational Chemistry: the first forty years*, ed. C. E. Dykstra, G. Frenking, K. S. Kim and G. E. Scuseria, Elsevier, 2005, pp.1167–1189.

[S6] Report for FMO: K. Kitaura, E. Ikeo, T. Asada, T. Nakano and M. Uebayasi, *Chem. Phys. Lett.*, 1999, **313**, 701–706.

[S7] Report for pair interaction energy decomposition analysis (PIEDA): D. G. Fedorov and K. Kitaura, *J. Comput. Chem.*, 2007, **28**, 222–237.

4. Solution-state behaviors

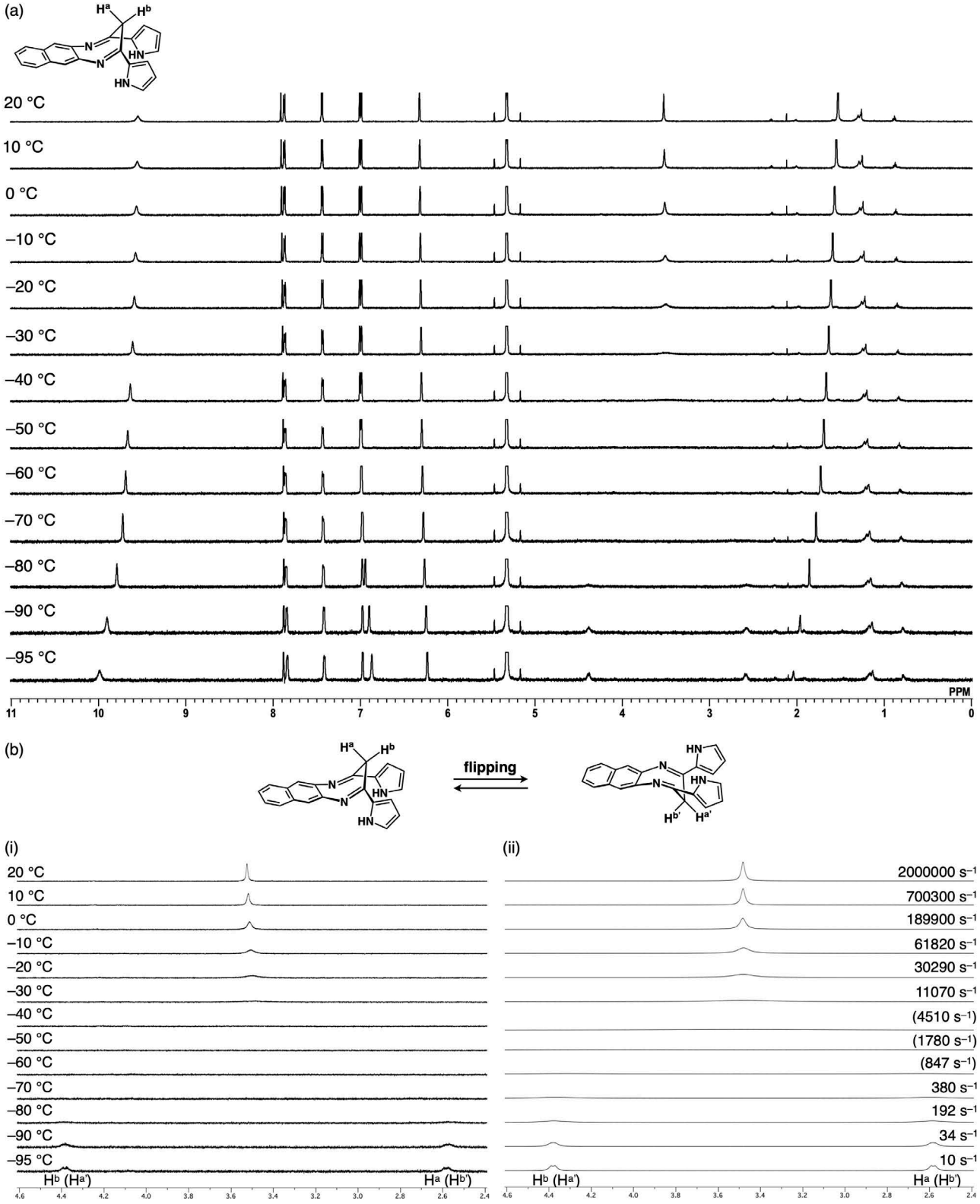

Fig. S32 (a) VT ^{1}H NMR spectra of **2a** in CD_2Cl_2 (1.0×10^{-3} M), (b)(i) enlarged spectra for methylene protons H^a and H^b and (ii) simulated ^{1}H NMR spectra[S8] for H^a and H^b, and (c) Eyring plot. The details on the observed $\Delta S^{\ddagger}$, which induces the faster flipping behavior, will be discussed elsewhere.

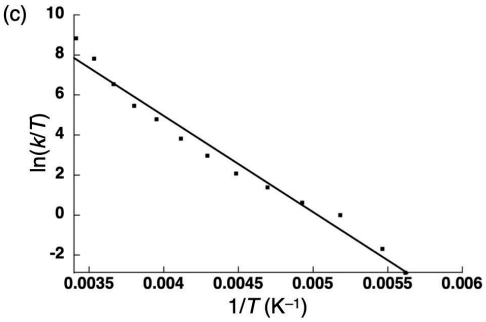

$\ln(k/T) = -4808.0(1/T) + 24.190$
$\Delta H^{\ddagger} = 40.0$ kJ mol^{-1} (9.56 kcal mol^{-1})
$\Delta S^{\ddagger} = 3.57$ J K^{-1} mol^{-1} (0.85 cal K^{-1} mol^{-1})
$\Delta G^{\ddagger} = 38.9$ kJ mol^{-1} (9.31 kcal mol^{-1}) at 293 K
(rate constant $k = 2000000$ s^{-1} at 293 K)

Fig. S32 (Continued)

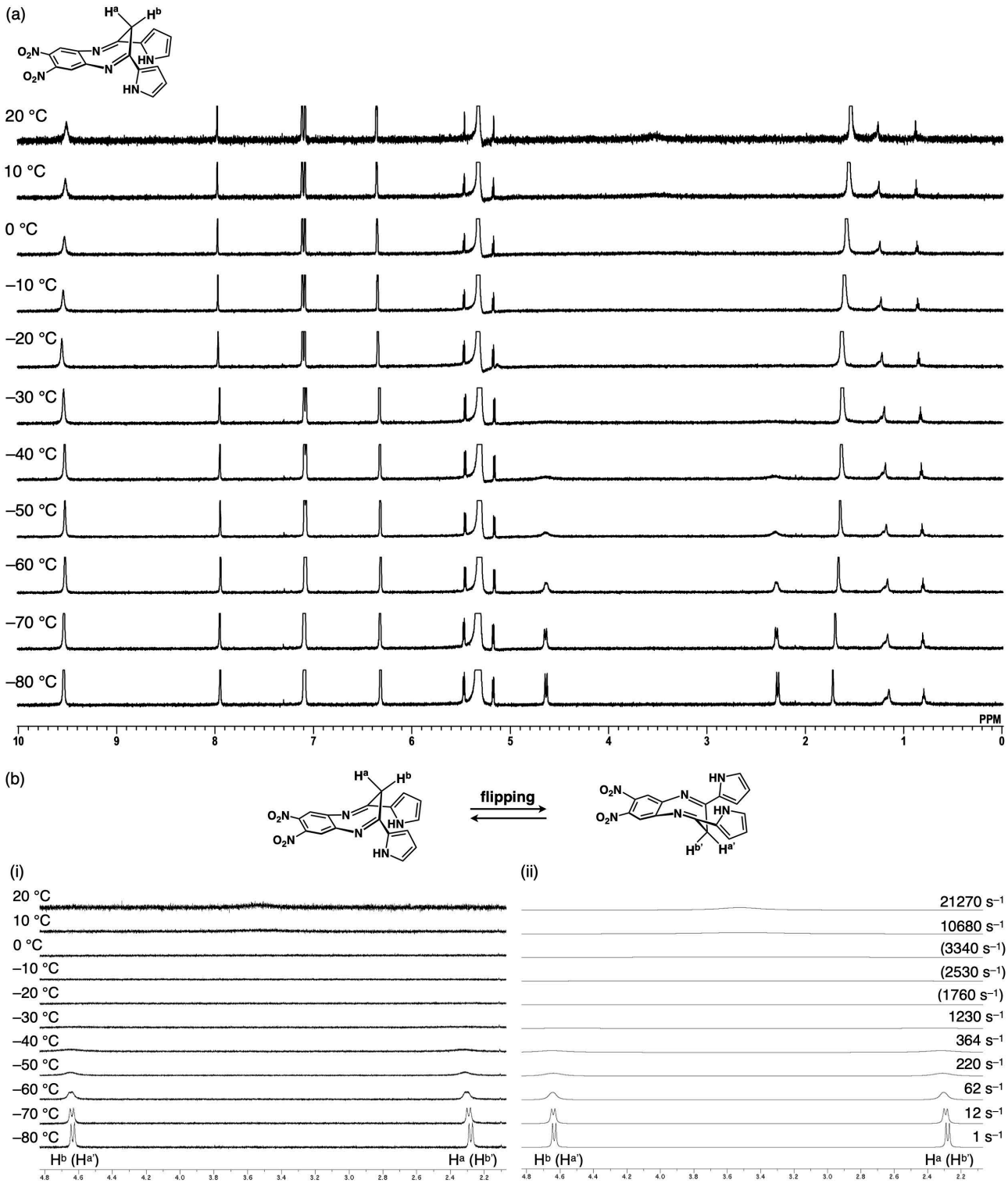

Fig. S33 (a) VT ^{1}H NMR spectra of **2b** in CD_2Cl_2 (1.0×10^{-3} M), (b)(i) enlarged spectra for methylene protons H^a and H^b and (ii) simulated ^{1}H NMR spectra[S8] for H^a and H^b, and (c) Eyring plot.

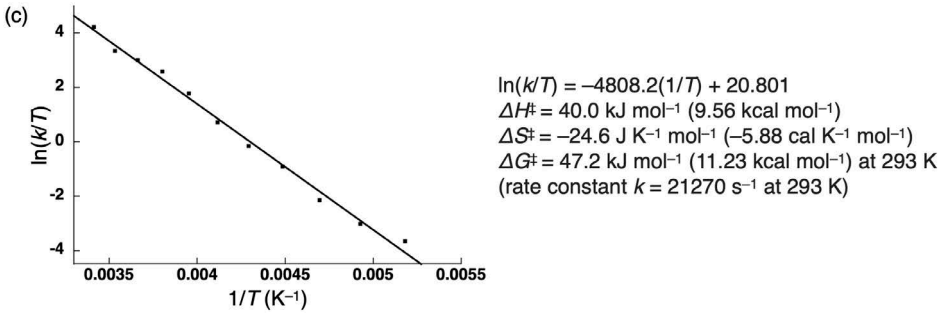

Fig. S33 (Continued)

[S8] *iNMR* ver. 5.0.1 (http://www.inmr.net).

5. Solid-state photophysical properties

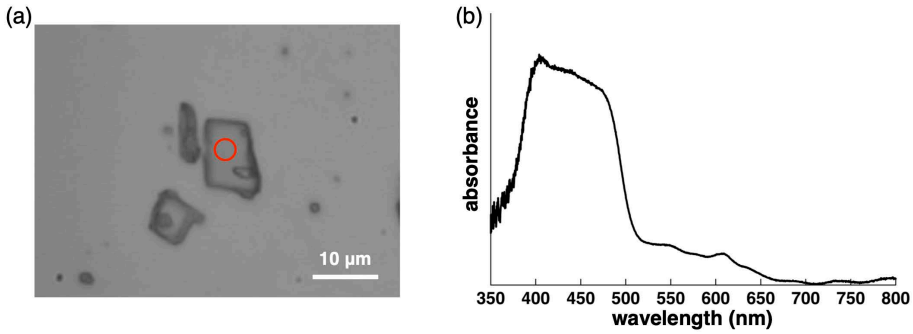

Fig. S34 (a) Optical microscopic image and (b) UV/vis absorption spectrum of single crystal of **2a**$_6$·C_{60}. Red circle indicates the position where the UV/vis absorption measurement was conducted. The large band at 400–500 nm, which was distinct from the UV/vis absorption bands of the dispersed **2a** and C_{60} in solution, can be derived from their charge-transfer interaction.

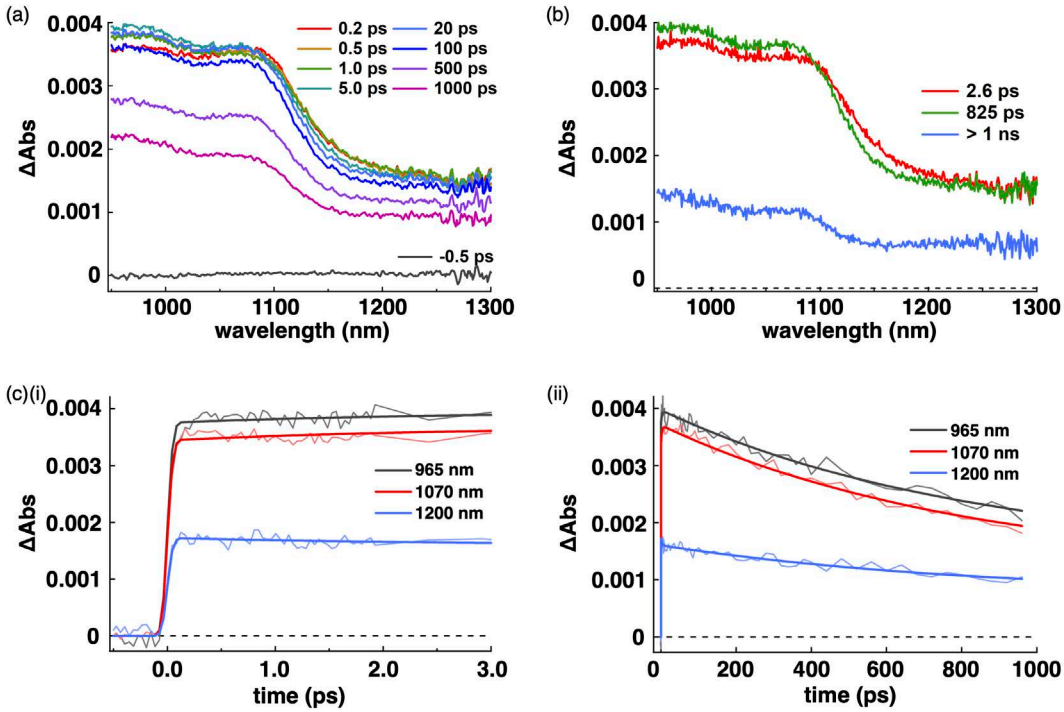

Fig. S35 (a) Sub-picosecond to nanosecond transient absorption spectra, (b) evolution-associated spectra (EAS) obtained by the global analyses with singular value decomposition (SVD), and (c,d) decay profiles of the transient absorbance at different probe wavelength of a single crystal of **2a**$_6$·C_{60} excited at 400 nm. The labels in (c) indicate the respective time constants (τ) of corresponding EAS of **2a**$_6$·C_{60} (2.6 ps: red; 825 ps: green; >1 ns (fixed): blue).

Molar absorption coefficients at 400 nm of **2a** (six units, CH_2Cl_2) and C_{60} (benzene)[S9] are 3.6×10^3 and 2×10^3 M^{-1} cm^{-1}, respectively. If we assume that the absorption spectrum of the single crystal of **2a**$_6$·C_{60} is expressed as the superposition of the six times of absorption spectrum of **2a** and the absorption spectrum of C_{60} in solutions, it is expected that the 400-nm laser pulse mainly excites **2a** in the **2a**$_6$·C_{60} assembly. Just after the excitation with a 400-nm pulse, a broad transient absorption band instantaneously appeared at ~965 and ~1070 nm in (a). It is noted that the shapes of the transient absorption spectra and dynamics were independent of the excitation intensity under the present excitation intensity, suggesting that nonlinear optical effects can be excluded. The transient absorption band at ~1070 nm can be ascribed to the C_{60} radical anion based on the assignments of previous reports.[S10] DFT calculations suggest that the direct charge-transfer (CT) transition appears near the band edge in **2a**$_6$·C_{60} (Fig. S22,27). Therefore, this result indicates that the ultrafast photoinduced electron transfer or direct CT transition takes place from **2a** to C_{60} within the instrumental response function (~100 fs). The transient absorption band at ~965 nm was not observed in the previous report.[S1] In addition, a broad absorption band over the NIR light region superposed on the absorption of the C_{60} radical anion. These signals may be assigned to the radical cation of **2a** and the refraction and scattering due to the change of refractive index of the crystal by the excitation. The three-state sequential kinetic model was assumed to obtain the evolution-associated spectra in (b). The spectral shape of the first EAS (τ = 2.6 ps) is similar but slightly broader than that of the second EAS (τ = 825 ps). Therefore, the first EAS is ascribable to the higher vibrational state of the lowest CT state and the time

constant indicates the vibrational cooling. In the process from the second to third EAS ($\tau > 1$ ns), the transient absorption band associated with the radical anion of C_{60} and that at ~950 nm, which may be ascribed to the radical cation of **2a** mostly decays and the broad transient absorption band remains. Therefore, the time constant of the second EAS may indicate the charge recombination. The third EAS ($\tau > 1$ ns) is composed of the broad transient absorption band and the small amount of the transient absorption band associated with the radical anion of C_{60}. The third EAS species may be ascribable to the superposition of the residual radical cations and anions survived from the geminate charge recombination and the triplet excited state of C_{60}.

While the electron transfer to C_{60} by photoexcitation has been reported in various host–guest systems, these time constants are larger than hundreds of femtoseconds or picoseconds. The reason for the ultrafast electron transfer in the single crystal of $\mathbf{2a}_6 \cdot C_{60}$ is most probably because of the proximity of the donor and acceptor due to the curved geometry of **2a** because the distance between the donor and acceptor directly affects the rate of the electron transfer and the electronic interaction. The direct CT transition estimated by DFT calculations (Fig. S27) may also play a crucial role in the ultrafast electron-transfer process of $\mathbf{2a}_6 \cdot C_{60}$.

Moreover, global analyses with SVD revealed that both the spectral shapes of the decay-time components of 2.6 ps and 825 ps are similar to that of the C_{60} radical anion. In addition, the spectrum of 2.6 ps is slightly broader than that of 825 ps. Therefore, the species of 2.6 ps can be ascribed to the higher vibrational state of the C_{60} radical anion, and the decay time of 2.6 ps indicates the vibrational cooling. The species of 825 ps can be ascribed to the ground state of the C_{60} radical anion in (b), and the decay time of 825 ps probably indicates the charge recombination. The evolution-associated spectrum whose time constant is >1 ns still shows the absorption of the C_{60} radical anion. The long lifetime component may be ascribable to the superposition of the residual radical cations and anions survived from the geminate charge recombination and the triplet excited state of C_{60}.

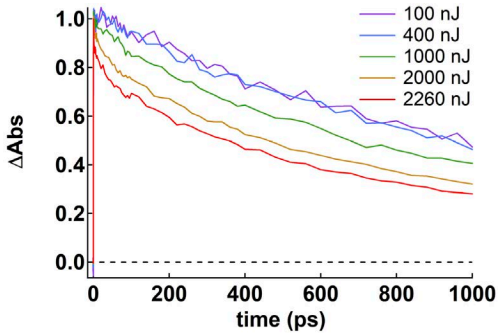

Fig. S36 Intensity-dependent transient absorption dynamics of a single crystal of $\mathbf{2a}_6 \cdot C_{60}$ excited and probed at 400 and 1070 nm, respectively. The shapes of the transient absorption spectra did not change irrespective of the excitation intensity. On the other hand, the fast decay components gradually appear with the increase in the excitation intensity. While the decay at 400 nJ pulse^{-1} has a slight fast decay component with a time scale of hundreds of picoseconds, the decay at 2260 nJ pulse^{-1} has clear and fast decay behavior. It is noted that the simple calculation suggests that the number of absorbed photons per single $\mathbf{2a}_6 \cdot C_{60}$ is smaller than 1 (1.1×10^{-1} photons per unit $\mathbf{2a}_6 \cdot C_{60}$ for 2260 nJ pulse^{-1}) (Fig. S35, which includes the detail of the calculations). Therefore, the intensity-dependent fast decay at the low excitation regime may suggest that transports of generated charges over multiple $\mathbf{2a}_6 \cdot C_{60}$ units in addition to the possibility of the single-singlet exciton annihilation.

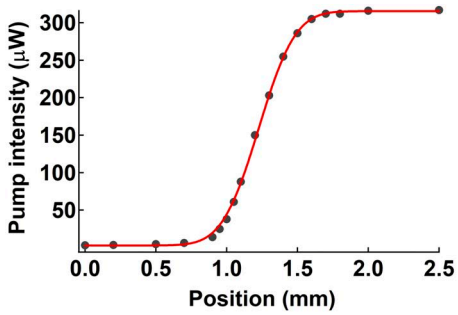

Fig. S37 Excitation intensity as a function of the relative position of the knife which blocks the excitation beam. The red line shows the fitting line with the error function. The number of photons supplied to a single unit of $\mathbf{2a}_6{\cdot}C_{60}$ was roughly estimated by using the absorption coefficients of **2a** (six units, CH_2Cl_2) and C_{60} (benzene)[S9] and the crystal structure of $\mathbf{2a}_6{\cdot}C_{60}$. The volume of the unit cell is calculated to be 6.22×10^{-24} L using lattice constants of $\mathbf{2a}_6{\cdot}C_{60}$. On the basis of the numbers of **2a** and C_{60} molecules of 12 and 2, respectively, in a unit cell, the numbers of **2a** and C_{60} per L in a crystal are 1.93×10^{24} and 3.21×10^{23}, respectively. Using the Avogadro constant, the molar concentrations of **2a** and C_{60} in a crystal can be calculated to be 3.30 and 0.534 M L^{-1}, respectively. The full width at the half maximum (FWHM) of the beam spot was experimentally measured to be 480 μm using the knife-edge method. When the excitation wavelength and intensity are 400 nm and 2 μJ $pulse^{-1}$, respectively, the excitation fluence was calculated to be 2.0×10^{-3} J cm^{-2}. The number of absorbed photons by a single $\mathbf{2a}_6{\cdot}C_{60}$ layer per unit area was estimated using the Lambert-Beer's law. Considering the probe pulse passing along the *a*- or *b*-axes of the crystal, the path length of a single $\mathbf{2a}_6{\cdot}C_{60}$ was assumed as the average of the lattice constants of *a* and *b*. Finally, the number of photons supplied to a single $\mathbf{2a}_6{\cdot}C_{60}$ unit was estimated to be 1.13×10^{-1} by multiplying the cross section of a single unit of $\mathbf{2a}_6{\cdot}C_{60}$, which was assumed to be the average of lattice constants of *a*- and *b*-axes. The estimated value is much smaller than 1, suggesting that $\mathbf{2a}_6{\cdot}C_{60}$ do not show any nonlinear photoresponses unless the photogenerated radical anions or cations (carriers) migrate over multiple $\mathbf{2a}_6{\cdot}C_{60}$ units. While the absorption coefficients of $\mathbf{2a}_6{\cdot}C_{60}$ would be underestimated because the electronic interaction of **2a** and C_{60} was not taken into account, this simple calculation suggests the potential of efficient carrier-transport property.

[S9] S. H. Gallagher, R. S. Armstrong, P. A. Lay and C. A. Reed, *J. Phys. Chem.*, 1995, **99**, 5817–5825.

[S10] (a) T. Kato, T. Kodama, T. Shida, T. Nakagawa, Y. Matsui, S. Suzuki, H. Shiromaru, K. Yamauchi and Y. Achiba, *Chem. Phys. Lett.*, 1991, **180**, 445–450; (b) T. Konishi, Y. Sasaki, M. Fujitsuka, Y. Toba, H. Moriyama and O. Ito, *J. Chem. Soc., Perkin Trans. 2*, 1999, 551–556.